# Influence of upper-ocean stratification on tropical cyclone-induced surface cooling in the Bay of Bengal

S. Neetu,[1] Matthieu Lengaigne,[1,2] Emmanuel M. Vincent,[2] Jérôme Vialard,[2] Gurvan Madec,[2,3] Guillaume Samson,[2] M. R. Ramesh Kumar,[1] and Fabien Durand[4]

[1] Surface cooling induced by tropical cyclones (TCs) is about three times larger during premonsoon than during postmonsoon season in the Bay of Bengal. We investigate processes responsible for this seasonal contrast using an ocean general circulation model. The model is forced by TC winds prescribed from an analytic vortex using observed TC tracks and intensities during 1978–2007. The simulation accurately captures the seasonal cycle of salinity, temperature, and barrier layer in this region, with fresher waters, deeper upper-ocean stratification, and thicker barrier layers during postmonsoon season. It also reproduces the three times larger TC-induced cooling during premonsoon than during postmonsoon season. This difference is essentially related to seasonal changes in oceanic stratification rather than to differences in TC wind energy input. During the postmonsoon season, a deeper thermal stratification combined with a considerable upper-ocean freshening strongly inhibits surface cooling induced by vertical mixing underneath TCs. On average, thermal stratification accounts for ∼60% of this cooling reduction during postmonsoon season, while haline stratification accounts for the remaining 40%. Their respective contributions however strongly vary within the Bay: haline stratification explains a large part of the TC-induced cooling inhibition offshore of northern rim of the Bay (Bangladesh-Myanmar-east coast of India), where salinity seasonal changes are the strongest, while thermal stratification explains all the cooling inhibition in the southwestern Bay. This study hence advocates for an improved representation of upper-ocean salinity and temperature effects in statistical and dynamical TCs forecasts that could lead to significant improvements of TC intensity prediction skill.

## 1. Introduction

[2] The Bay of Bengal (BoB) is home to about four named tropical cyclones (TCs) each year, which accounts for ∼5% of the total annual TC numbers worldwide [*Alam et al.*, 2003]. These few TCs may not be the most intense but have catastrophic impacts. Of the top 20 deadliest TCs in the world history, 14 were generated in the BoB [*Longshore*, 2008]. The high population density distributed along low-lying coastal areas and poor disaster management strategies largely explain this very strong vulnerability of countries around the Bay (India, Sri Lanka, Bangladesh, Myanmar) to

natural disasters. For instance, recent TC Nargis reached Category 4 strength and caused the worst natural disaster in Myanmar with more than 140,000 lives lost, one million homeless people, and over $10 billion in economic losses [*Webster*, 2008; *McPhaden et al.*, 2009]. It is therefore of utter practical importance to identify the key factors that control TC intensity in this region.

[3] Uncertainties in TC intensity forecasts are mainly related to three key factors: storm inner core dynamics, structure of the atmospheric synoptic scale environment, and interactions with upper-ocean layers [*Emanuel*, 1999; *Marks and Shay*, 1998]. This pivotal role of the ocean-atmosphere interaction arises from the fact that TCs primarily draw their energy from evaporation at the ocean surface [*Riehl*, 1950]. TCs generally cool the ocean surface by several degrees along their track [*Leipper*, 1967, *Shay et al.*, 1992, *Cione et al.*, 2000; *D'Asaro*, 2003]. While higher ambient SSTs provide the potential for stronger TCs, cyclone intensity is most sensitive to SST cooling under the storm eye [*Schade*, 2000]. This cooling reduces the total enthalpy flux provided to the atmosphere and inhibits the cyclone intensification [*Cione and Uhlhorn*, 2003]. While energy input associated

---

[1]National Institute of Oceanography, Goa, India.
[2]LOCEAN, Institut Pierre Simon Laplace, Paris, France.
[3]National Oceanographic Centre, Southampton, UK.
[4]Laboratoire d'Etudes en Géophysique et Océanographie Spatiale, Observatoire Midi Pyrénées, Toulouse, France.

Corresponding author: S. Neetu, National Institute of Oceanography, Dona Paula, 403004 Goa, India. (neetu@nio.org)
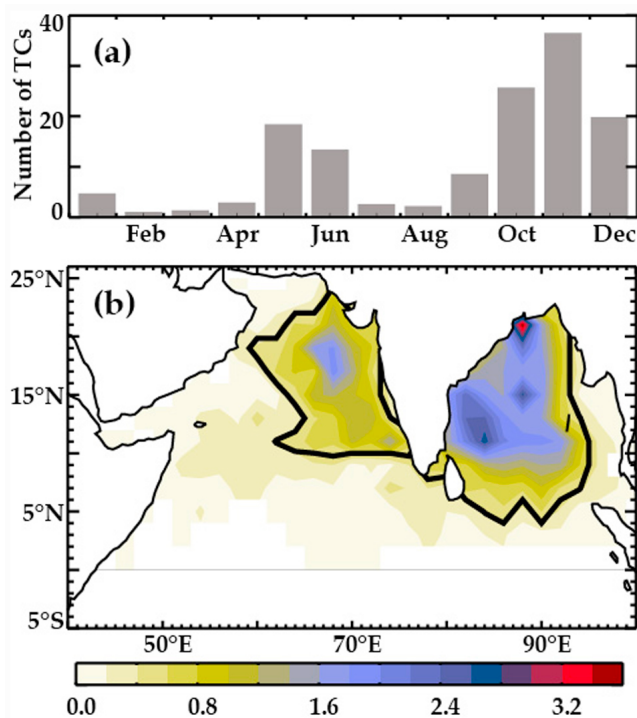
**Figure 1.** (a) Seasonal evolution of the number of TCs north of the equator in the Indian Ocean over the 1978–2007 period. (b) Number of TCs per year in 2° by 2° bins over the 1978–2007 period. The thick 0.4 isoline delineates a region where 80% of TCs occur in the northern Indian Ocean. Data set used is the International Best Track Archive for Climate Stewardship (IBTrACS) [Knapp et al., 2010].

with TC winds is the key factor controlling the amplitude of TC-induced cooling [e.g., Vincent et al., 2012a, hereafter V12a], several studies have also illustrated the influence of subsurface oceanic background conditions on the TC-induced SST signature [Shay et al., 2000; Cione and Uhlhorn, 2003; Jacob and Shay, 2003; Shay and Brewster, 2010; Lloyd and Vecchi, 2011; Vincent et al., 2012b]. Vincent et al. [2012b, hereafter V12b] indeed showed that the widely varying upper-ocean precyclone stratification could modulate TC-induced cooling amplitude by up to an order of magnitude for a given level of TC kinetic energy input to the upper ocean. The impact of oceanic stratification on TC intensification has recently been illustrated within the BoB [Ali et al., 2007]. In the case of TC Nargis, Yu and McPhaden [2011] highlighted the apparent connection between a high temperature, a low salinity front, and the TC intensity, suggesting a tight coupling between the cyclone and the ocean stratification.

[4] In the BoB, TCs mainly occur in the western and central part of the basin (Figure 1b) and have a bimodal distribution (Figure 1a): they preferentially occur during the premonsoon and postmonsoon seasons. These TCs are promoted by high sea surface temperatures (SSTs), a dynamically unstable atmosphere and low tropospheric wind shear during the postmonsoon/premonsoon season while they are inhibited by strong tropospheric wind shear during the monsoon [Menkes et al., 2012]. The BoB SST remains above the 28°C threshold in all seasons. Compared to other

TC-prone regions, the BoB has a very peculiar oceanic stratification. It indeed displays a strong near-surface halocline with very low salinity in the northeastern part of the basin and higher salinity in the southwest [e.g., Rao and Sivakumar, 2003]. The fresher surface salinity in the northern part of the Bay largely results from oceanic rainfall and from the huge river discharges [Sengupta et al., 2006; Shetye et al., 1996]. The oceanographic characteristics of the BoB also undergo seasonal changes in response to the wind and freshwater forcing fluxes associated with the monsoon. Mixed-layer temperature drops by about 1°C during summer monsoon, as a result of reduced shortwave radiation and increased latent heat loss [Shenoi et al., 2002; De Boyer Montégut et al., 2007a]. The excess precipitation and huge river runoff during summer monsoon lead to low-salinity water in the vicinity of river mouths in the northern BoB, which is then advected into the southern BoB [Vinayachandran et al., 2005] and eastern Arabian Sea by the East India Coastal Current [Shetye et al., 1991; Shenoi et al., 2005; Kurian and Vinayachandran, 2007; Durand et al., 2007]. In addition, a substantial amount of low-salinity water escapes from the BoB along the eastern boundary [e.g., Han and McCreary, 2001; Sengupta et al., 2006]. This results in a very strong near-surface halocline along the rim of the BoB during the postmonsoon season, which affects density stratification and the depth of wind-induced vertical mixing [Vinayachandran et al., 2002]. As a consequence, the mixed layer is usually shallow there and controlled by salinity stratification. This often results in the formation of a barrier layer (BL) [Lukas and Lindstrom, 1991; Sprintall and Tomczak, 1992], the layer between the base of the mixed layer and the top of the thermocline. The BL that forms during summer monsoon in the northern bay exists throughout the postmonsoon season but is much thinner during the premonsoon season [Thadathil et al., 2007]. This BL prevents turbulent entrainment of cooler thermocline water into the mixed layer and consequently maintains warm SST. This largely explains why SST and sea level anomalies are less correlated in the BoB than in other basins [Gopalan et al., 2000; Rao and Behera, 2005].

[5] Previous studies suggest that those seasonal stratification changes modulate the amplitude of TC-induced surface cooling. Indeed, SST cooling underneath TCs is larger during premonsoon (∼2–3°C) [Gopalakrishna et al., 1993; Rao, 1987; Sengupta et al., 2008] than during postmonsoon season in the BoB (∼0.5°–1°C) [Chinthalu et al., 2001; Sengupta et al., 2008; Subrahmanyam et al., 2005]. From oceanic observations for individual case studies, Sengupta et al. [2008] suggested that the weaker observed surface cooling during the postmonsoon season results from the presence of the BL that prevents entrainment of cold water into the mixed layer. These findings led the authors to speculate that freshwater from monsoon rain and river runoff may influence TC intensity in the BoB.

[6] The aforementioned study relies on a restricted number of TCs (eight) and CTD data over a short period (October 2003), which prevented the authors from providing a quantitative estimate of the respective influences of the seasonal changes in haline and thermal stratification on the differences in TC-induced cooling amplitude between the two seasons. In the present paper, we address this issue using a much larger sample. This is made possible by the use

of V12a's global ocean simulation which includes TC wind-forcing prescribed from an analytical vortex fitted to observed TC tracks and intensities over the 1978–2007 period. This simulation captures reasonably well the main characteristics of TC-induced surface cooling at the global scale [V12a]. Our approach hence provides a relatively large sample consisting of the simulated oceanic response to 135 TCs over a 30-year period in the BoB. While V12b discuss the sensitivity of TC-induced cooling amplitude to the precyclone stratification at global scale, it neither discusses regional aspects nor the potential salinity contribution to the upper-ocean stratification. The present paper hence allows investigating TC surface response in a region where salinity stratification is known to be particularly strong and has hence been suggested to influence TC-induced cooling amplitude.

[7] The paper is organized as follows. Section 2 briefly describes the observational data sets as well as our numerical strategy. Section 3 validates the model climatology and cold wake characteristics for the premonsoon and post-monsoon seasons. We then analyze and relate differences in TC-induced cooling between the two seasons to the thermohaline stratification in section 4 and further quantify the respective contributions of temperature and salinity stratification to TC-induced cooling amplitude. The final section provides a summary of our results and a discussion of their implications.

## 2. Data and Methods

### 2.1. Observed Data Sets

[8] We use the temperature and salinity of the North Indian Ocean Atlas (NIOA) [*Chatterjee et al.*, 2012] to validate the model climatological thermohaline structure in the BoB. This monthly climatology of $1° \times 1°$ spatial resolution uses all the data accounted for in the World Ocean Atlas 2009 [*Locarnini et al.*, 2010; *Antonov et al.*, 2010] but adds a considerable amount of data from Indian sources, especially within the Indian Exclusive Economic Zone. This addition improves considerably the climatology in the BoB compared to the WOA, especially along its western boundary [*Chatterjee et al.*, 2012]. We also validate the simulated mixed layer depth (MLD) and BL thickness (BLT) with the updated MLD climatology and BLT climatology of *de Boyer Montégut et al.* [2004, 2007b], which now includes ARGO profiles until September 2008.

[9] We use the blended Tropical Rainfall Measuring Mission (TRMM) Microwave Imager (TMI) and Advanced Microwave Scanning Radiometer (AMSR-E) SST daily data set (available from http://www.ssmi.com/sst/microwave_oi_sst_data_description.html) at $0.25° \times 0.25°$ spatial resolution to characterize the observed SST response to TCs over the 1998–2007 period and validate the simulated one. Despite their inability to retrieve SST data under heavy precipitation, TMI and AMSR-E offer the advantage of being insensitive to atmospheric water vapor and provide accurate observations of SST beneath clouds [*Wentz et al.*, 2000], a few days after (and before) TC passage. The inner-core cooling (i.e., cooling underneath the eye) cannot be assessed confidently with TMI-AMSR-E, since data are most of the time missing within 400 km of the current TC position. This data set however provides a reliable estimate

of the cooling in the TC wake, valid data being typically available 1 to 2 days after TC passage.

[10] Observed TC position and magnitude are derived from the International Best Track Archive for Climate Stewardship (IBTrACS) [*Knapp et al.*, 2010]. In this study, we focus on the 1978–2007 period, over which global satellite coverage provides the position and estimated maximum wind speed every 6 h for more than 3000 TCs worldwide (135 in the BoB). To define the premonsoon and the postmonsoon seasons, we consider the months when more than five TCs occurred during the 1978–2007 period (Figure 1a). May–June will then be considered as the premonsoon season and September–October–November–December as the postmonsoon season. It should however be noted we defined those periods based on cyclonic seasons rather than traditional monsoon (the months of June and September being usually encompassed within the monsoon period [*Wang et al.*, 2009]).

### 2.2. Model Description and Setup

[11] The model configuration and strategy to include TC forcing have been previously described in V12a. The following section provides a short summary of this modeling framework.

[12] We use a $1/2°$ global ocean model configuration (known as ORCA05 [*Biastoch et al.*, 2008a]) built from the Nucleus of European Model of the Ocean (NEMO), version 3.2 [*Madec*, 2008], with 46 vertical levels (10 levels in the upper 100 m and 250 m resolution at depth). This configuration includes the latest version of mixed layer dynamics: a turbulent kinetic energy (TKE) closure scheme [*Blanke and Delecluse*, 1993] improved by including the effect of Langmuir cells [*Axell*, 2002], a surface wave breaking parameterization [*Mellor and Blumberg*, 2004], and an energetically consistent time and space discretization [*Burchard*, 2002; *Marsaleix et al.*, 2008]. This configuration successfully reproduces Indo-Pacific ocean variability from interannual to decadal time scales [*Penduff et al.*, 2010; *Lengaigne et al.*, 2012; *Keerthi et al.*, 2012; *Nidheesh et al.*, 2012] as well as the local SST response to TC wind-forcing [V12a].

[13] In this configuration, the MLD is defined as the depth where density is 0.01 kg.m$^{-3}$ higher than surface density. The different terms contributing to the heat budget in the ocean mixed layer (ML) are calculated online, stored as daily averages, and provide the following closed budget for the ML temperature evolution:

$$\partial_t T = -\underbrace{\langle u\partial_x T + v\partial_y T + w\partial_z T\rangle}_{a} + \underbrace{\langle D_l(T)\rangle}_{b} - \underbrace{\frac{1}{h}\frac{\partial h}{\partial t}(T - T(z=h))}_{c}$$
$$+ \underbrace{\frac{(k\partial_z T)(z=h)}{h}}_{d} + \underbrace{\frac{Q^* + Q_s(1 - F(z=h))}{\rho_0 C_p h}}_{e} \quad (1)$$

where $T$ is the model temperature in the ML, $(u, v, w)$ are the components of ocean currents, $D_l(T)$ is the lateral diffusion operator, $k$ is the vertical diffusion coefficient, and $h$ is the time varying MLD. Brackets denote the vertical average over the mixed layer $h$ and a is the advection, b is the lateral diffusion, c is the entrainment/detrainment at the ML base, d is the vertical diffusion flux at the ML base, and e is heat flux storage in the ML (with $Q_s$ the solar heat flux and $Q^*$
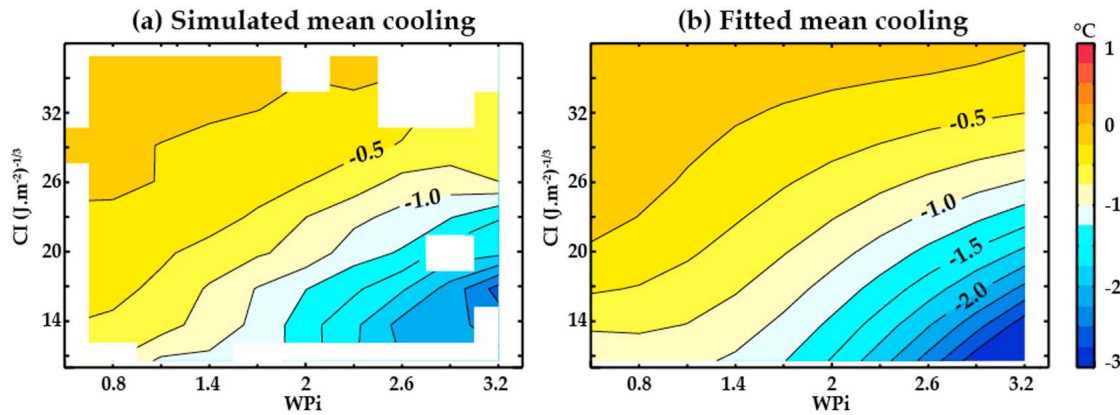
**Figure 2.** (a) Average TC-induced cooling in the model in the BoB, as a function of the WPi (a proxy of the TC-energy input into the upper ocean, see text for details) (10 bins of 0.3) and CI (a proxy of the inhibition of the cooling by the ocean stratification, see text for details) (10 bins of 3). Bins with less than six samples are shaded in white. (b) Best fit of the model cooling using degree 2 polynomial.

the nonsolar heat fluxes: sensible, latent, radiative heat fluxes; $F(z = h)$ is the fraction of surface solar irradiance that penetrates below the mixed layer.

[14] As in V12a, we will use this heat budget calculation to infer the respective contribution of these processes to the amplitude of TC-induced cooling. The term b for lateral diffusion is negligible in the wake of TCs (not shown). In the following, b is neglected, c and d are grouped together in a vertical processes term and referred to as MIX; e the surface forcing term is referred to as FOR; a the advection term is referred to as ADV. To quantify the relative contribution of all processes to the cooling magnitude, each term of the ML heat budget is integrated starting 10 days prior to TC passage.

[15] The simulations analyzed in this paper use the atmospheric data sets and formulations proposed by *Large and Yeager* [2009] as surface boundary conditions. This approach was developed in the design of the "coordinated ocean-ice reference experiments (COREs)" program [*Griffies et al.*, 2009] and is referred to as CORE II forcing. The forcing data sets presented by *Large and Yeager* [2009] are based on NCEP/NCAR reanalysis for near-surface wind, temperature, specific humidity, and density, combined with a variety of satellite data sets for radiation, SST, sea-ice concentration, and precipitation. Turbulent fluxes are computed from bulk formulae as a function of the prescribed near-surface atmospheric state and the simulated ocean surface state (SST and surface currents). Data are provided at 6-hourly (wind speed, humidity, and atmospheric temperature), daily (short- and long-wave radiation), and monthly (precipitation) resolution, with interannual variability over the 1978–2007 period except for river runoff that remains climatological [*Fekete et al.*, 2002]. To avoid an artificial model drift, the sea surface salinity is nudged toward monthly mean climatological values with a 300 days relaxation timescale (for a 50-m-thick mixed layer) [*Griffies et al.*, 2009]. The large nudging timescale compared to the typical response time to a TC allows simulating a realistic climatological haline stratification, a key feature to study the TC ocean response in the Bay, without significantly affecting the salinity stratification at the timescale of TCs (a few days). The model starts from an ocean at rest

initialized with temperature and salinity fields from the World Ocean Atlas 2005 [*Locarnini et al.*, 2006; *Antonov et al.*, 2006]. It is then spun up for a 30-year period using the CORE II bulk formulae and interannual forcing data set (1948–1977) [*Large and Yeager*, 2009; *Griffies et al.*, 2009]. The final state is then used to start the simulations described below (which are run over 1978–2007).

[16] The NCEP/NCAR reanalysis used as wind-forcing in the original CORE II data set has a coarse horizontal resolution (∼2°), insufficient to resolve the spatial scale of TCs that typically display radius of maximum wind of ∼50 km [*Kikuchi et al.*, 2009]. This data set hence only contains weaker-than-observed TC wind signatures (TC-like vortices) and cannot directly be used to investigate the model response to TCs, as shown by V12a. To include a more realistic TC wind-forcing, a cyclone-free forcing is first prepared from the original interannual CORE II forcing by filtering these TC-like vortices. These residual TC signatures have been filtered out by applying a 11-day running mean (the maximum time of influence of a TC at a given point) to the zonal and meridional wind components of the original CORE II wind-forcing, within 600 km around each cyclone track position, with a linear transition from filtered to unfiltered winds between 600 and 1200 km (the maximum radius of influence for TC winds). A new forcing is then constructed with realistic TC-wind signatures superimposed on the filtered forcing. The 6-hourly cyclone position and magnitude from IBTrACS database [*Knapp et al.*, 2010] are linearly interpolated onto the model grid and timestep (i.e., every 36 min). This information is used to reconstruct the 10-m wind vector from an idealized TC wind vortex fitted to observations (*Willoughby et al.* [2006]; see their Figure 2 for the resulting analytical wind profile). This procedure results in a simulation where TC wind magnitude and structure is more realistic than in the CORE II original forcing (see Figure 1 in V12a). A more detailed description of this forcing strategy can be found in V12a, together with a model validation at global scale. Similar strategies have been recently successfully used to assess the impact of TCs in the ocean [*Wang et al.*, 2012a, 2012b]. *Vincent et al.* [2012c] further showed that the 1/2° resolution is a good compromise

between accuracy and numerical cost for a realistic global simulation of the ocean response to TCs: compared to a 1/12° grid, a 1/2° resolution provides very similar results in terms of TC power dissipation, a good proxy for TC-induced vertical mixing, while slightly underestimating the TC wind-driven upwelling.

## 2.3. Methodology to Monitor the Ocean Response

[17] To characterize the ocean response to TCs, we first subtract the mean SST seasonal cycle from the model and TMI-AMSR-E observations. This mean seasonal cycle is calculated over 1998–2007 when comparing model results to observations (Figures 7 and 8) and over 1978–2007 when model results are extended over the entire available period (Figure 9 onward). TC track locations are then used to retrieve the ocean response to TCs. Average SST anomalies within a fixed radius of 200 km (about 4 radii of maximum wind) around each TC track position are used to characterize the cooling amplitude. This scale corresponds to the area where SST is known to influence TC intensity [Cione and Uhlhorn, 2003; Schade, 2000].

[18] Following V12a, the reference unperturbed prestorm SST conditions ($SST_0$) are defined as the 7-day average ending 72 h before the TC passage while the SST in the cold wake (CW) of the TC ($SST_{CW}$) is defined as the 3-day average starting 24 h after the storm passage. The amplitude of the SST response is characterized by the cooling amplitude in the CW as $\Delta T_{CW} = SST_{CW} - SST_0$. We will see in section 3 and specifically from Figure 7 that these choices for temporal averaging are justified by our observational and modeling results.

[19] Following V12b, two variables are used in this study to diagnose the TC atmospheric forcing magnitude and the influence of subsurface oceanic background conditions. The Wind Power index (WPi) characterizes the strength of TC forcing. It integrates several parameters known to influence the CW amplitude (storm size, maximum winds, and translation speed of the TC) in a single measure. The WPi builds on the power dissipated ($PD$) by friction at the air-sea interface [Emanuel, 2005] that is a good proxy of the kinetic energy transferred from the winds to the ocean surface currents [V12b]. The $PD$ is calculated for each cyclone track position as

$$PD = \int_{t_b}^{t_a} \rho \, C_D |\mathbf{V}|^3 \, dt \qquad (2)$$

and the WPi is obtained as follows:

$$WPi = [PD/PD_0]^{1/3} \qquad (3)$$

where $|\mathbf{V}|$ is the local magnitude of surface wind, $C_D$ is the dimensionless surface drag coefficient, $\rho$ is the surface air density, $t_b$ is the time when a cyclone starts influencing the considered location, and $t_a$ is the time after the cyclone passage; $PD = \int_{t_o}^{t_c} \rho C_D |\mathbf{V}|^3 dt$ is a normalization constant corresponding to a weak storm with a translation speed of 7 m s$^{-1}$ (25 km h$^{-1}$) and a maximum 10-min averaged wind speed of 15 m s$^{-1}$ (the wind speed defining a Tropical Depression: the weakest classified cyclonic system). Here $t_b$ is set to 3 days before a TC reaches a given ocean point,

while $t_a$ is taken as 3 days after the TC passage. As discussed in V12a, results are rather insensitive to reasonable changes of these parameters.

[20] WPi is a proxy of the amount of kinetic energy available for mixing underneath the storm [V12b]. As cooling mainly results from mixing induced by the vertical shear of oceanic currents [Price, 1981; V12a], WPi is hence a pertinent variable to describe the former. V12b have shown that the mean cooling underneath a TC increases nearly linearly with WPi but demonstrated that the cooling magnitude also depends on ocean background conditions.

[21] In addition to this atmospheric variable, we hence use an oceanic variable, the Cooling Inhibition index (CI), also introduced by V12b, which characterizes the ocean background conditions control of the cooling amplitude. This index is based on the physical process responsible for the cooling: conversion of kinetic energy to potential energy by vertical mixing. V12b show that the amplitude of the cooling is proportional to the cube root of the potential energy change. CI is hence defined as the cube root of the potential energy necessary to produce a 2°C surface cooling via vertical mixing:

$$CI = \left[\Delta E_p(-2°C)\right]^{1/3} \text{ with } \Delta E_p(\Delta T) = \int_{h_m}^{0} \left(\rho_f - \rho_i(z)\right) g z \, dz$$

(4)

where $g$ is the acceleration of gravity, $z$ is ocean depth, $\rho_i$ is the pre-cyclone density profile, $\rho_f$ is the homogeneous final density profile, and $h_m$ is the mixing depth allowing a 2°C surface cooling via a heat-conserving mixing.

[22] This quantity can easily be computed from any available temperature and salinity profiles before the cyclone passage (by assuming that mixing results in a perfectly homogeneous temperature and salinity profile). It measures the inhibition of mixing-induced surface cooling by the ocean background state. CI is a good measure of this inhibition because it integrates two relevant parameters for the cooling amplitude: the MLD before the cyclone passage, and the strength of the stratification underneath this mixed layer. Indeed, the deeper the initial mixed layer, the more kinetic energy is required to produce mixing at its base. And the deeper the initial mixed layer, the greater the thermal capacity of the surface layer: for a given available energy, a thicker layer cools less. The stratification at the base of the mixed layer is another relevant parameter because it sets the temperature of water that can be entrained into the mixed layer during mixing. The CI is computed from both temperature and salinity profiles and therefore accounts for the intensity of the haline stratification, including BL effect in its calculation.

[23] V12b showed that TC-induced SST variations in our simulation are largely a function of WPi and CI, with CI modulating the cooling amplitude by up to an order of magnitude for a given WPi. The dependence of the cooling amplitude on both WPi and CI for the specific case of the BoB is further illustrated on Figure 2a where the average cooling amplitude underneath TC conditions in the Bay is binned as a function of WPi and CI. The average cooling increases as a function of *WPi* and decreases as a function of CI. Large cooling (>2°C) only occurs in the BoB when
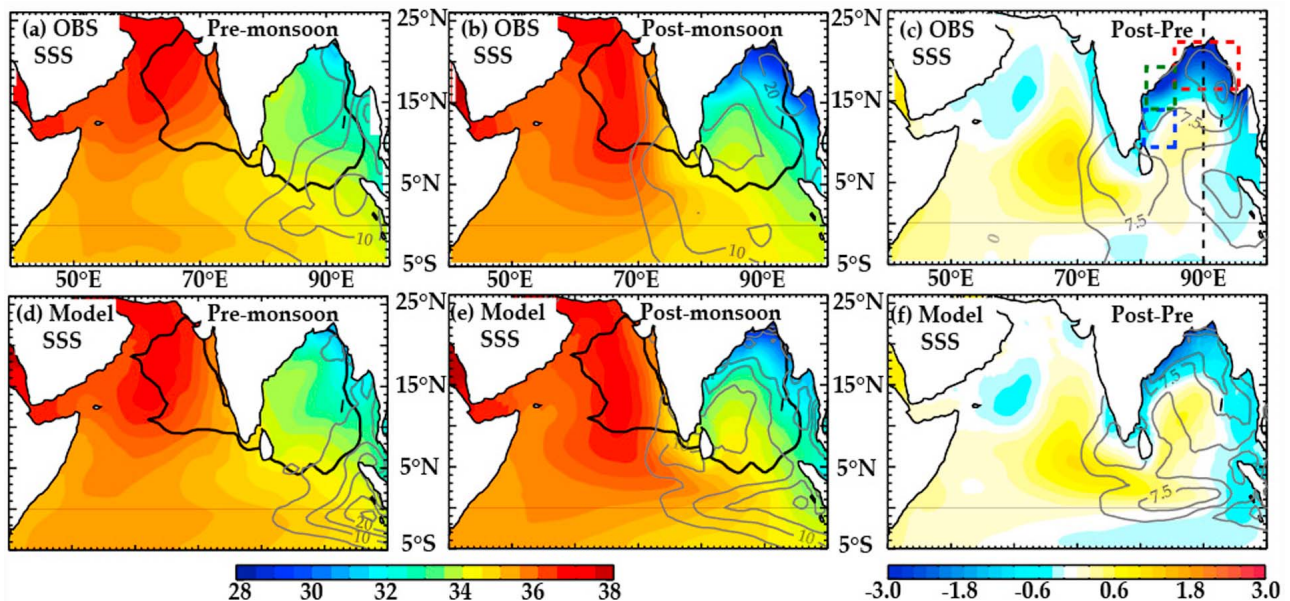
**Figure 3.** Climatological SSS (in psu; color) and BLT (in meters, gray contours, 5 m contour intervals) for (a and d) premonsoon and (b and e) postmonsoon seasons and (c and f) their difference derived from observed SSS climatology of *Chatterjee et al.* [2012] and (top) BLT climatology of *De Boyer Montégut et al.* [2004] and (bottom) model over the 1978–2007 period. The thick contour on Figures 3a, 3b, 3d, and 3e delineates a region where 80% of TCs occur in the northern Indian Ocean (see Figure 1). Dashed colored boxes on Figure 3c highlight the regions of the BoB discussed in Table 1 (red: northeast BoB, green: east Indian Coast, blue: southwest BoB). The black dashed line indicates the temperature and salinity section at 90°E shown on Figure 5.

powerful TCs (WPi > 2.5) travel over favorable oceanic conditions (CI < 20). As shown on Figure 2b, this dependence of the cooling amplitude on CI and WPi can be reasonably well approximated by a second-order polynomial least squares function. This least squares fit will be used in section 4 to hindcast the simulated cooling in the BoB and assess the respective contribution of thermal and haline stratification to TC-induced cooling amplitude.

[24] In order to assess the robustness of the results in this paper, we have performed significance tests on the differences between premonsoon and postmonsoon seasons in terms of mean state model oceanic changes (right sides of Figures 3, 4, 5, 6, and 11) as well as model and observed coolings under TCs (Figures 7, 8, 9, 13, and 14) using two-tailed Student tests and Mann-Whitney rank tests. All the differences that are discussed in the following are statistically significant at the 95% confidence level, except when stated otherwise.

## 3. Model Validation

[25] Figure 3 compares the model climatological sea surface salinity (SSS) with observational estimates for premonsoon and postmonsoon seasons in the northern Indian Ocean. In observations, high salinities characterize the Arabian Sea, due to the excess of evaporation over precipitation [*Rao and Sivakumar*, 2003] and proximity to two high-salinity seas, namely the Red Sea and the Persian Gulf. On the other hand, the BoB exhibits a large excess of precipitation over evaporation [*Harenduprakash and Mitra*, 1988; *Prasad*, 1997]. Low salinity water fills the entire bay

throughout the year, with freshest water along the coast adjacent to the major river mouths (Ganga, Brahmaputra, and Irrawadi). This results in a very large meridional salinity gradient, with very low salinity in the northern and eastern BoB and higher salinity in the southwestern BoB. Huge river runoff and excess precipitation over evaporation during summer monsoon lead to a postmonsoon near-surface salinity minimum of less than 28 psu in the northern part of the Bay (Figure 3b), 3 psu fresher than during the premonsoon season (Figure 3a). These regional patterns and seasonal features are reasonably well reproduced by the model (Figures 3d and 3e). The freshening of the Northern Bay may however be underestimated away from the coast during the postmonsoon season by ~1 psu (Figures 3c and 3f, Table 1), although observational estimates in this region may not be reliable due to the scarcity of available observations. If real, this underestimation may arise from inaccurate runoffs and precipitation forcing or from the rather coarse 1/2° resolution of the model that may not allow exporting enough coastal freshwater offshore.

[26] These low SSS in the BoB during postmonsoon season are associated with the development of a BL along the northern rim of the Bay, especially in the eastern part of the basin and along the eastern coast of India (Figures 3a and 3b, contours), in agreement with the observational analysis of *Thadathil et al.* [2007]. These BL are almost absent during the premonsoon season, except in the eastern part of the Bay where TCs hardly occur (Figure 3, thick contour). The model is also able to represent this seasonal contrast albeit with an underestimation of the BL spatial extent in the

**Table 1.** Average Observed and Modeled Differences Between Postmonsoon and Premonsoon Seasons for SSS, $H_{SST-2°C}$, BLT, and CI in the Regions Displayed as Colored Dashed Squares on Figures 3, 4, and 6[a]

| Regions | $\Delta$SSS (psu) | | $\Delta H_{SST-2°C}$ (m) | | $\Delta$BLT (m) | | $\Delta$CI $(J/m^2)^{1/3}$ | |
|---|---|---|---|---|---|---|---|---|
| | OBS | MOD | OBS | MOD | OBS | MOD | OBS | MOD |
| Northeast BoB | −2.2 | −1.3 | 13.0 | 15.6 | 14.3 | 11.9 | 8.4 | 9.0 |
| Southwest BoB | −0.2 | 0.0 | −6.6 | −1.8 | 6.3 | 2.4 | −1.4 | −0.9 |
| East Indian Coast | −1.5 | −1.0 | 4.0 | 14.0 | 9.8 | 8.8 | 3.6 | 5.0 |

[a]Northeast (85°E–95°E, 16°N–22°N), southwest (81°E–85°E, 9°N–14°N), and east Indian Coast (81°E–85°E, 14°N–20°N).

central and southwestern part of the Bay during postmonsoon season (Figures 3d–3f and Table 1).

[27] The near surface thermal stratification is diagnosed in the model and observations by calculating the depth at which ocean temperature is 2°C below the surface temperature ($H_{SST-2°C}$), a measure first proposed by *Lloyd and Vecchi* [2011]. The larger this depth the more difficult it is for a given TC to cool the ocean surface: it is thus an appropriate measure to validate the ocean thermal stratification in relation to TC response. Figure 4 compares the model climatological $H_{SST-2°C}$ with observational estimates for premonsoon and postmonsoon seasons in the Northern Indian Ocean, as well as the difference between the two seasons. Observations indicate that $H_{SST-2°C}$ is relatively homogeneous in the Bay during the premonsoon season (Figure 4a) but displays a clear east/west contrast during the postmonsoon season (Figure 4b). The upper-ocean stratification deepens by 20 to 30 m in the northeastern part of the Bay as well as by ∼10 m along the eastern coast of India (Figure 4c; Table 1). In contrast, the upper-ocean stratification shoals by ∼5–10 m in the southwestern part of the Bay. Seasonal $H_{SST-2°C}$ changes generally agree between model

and observations (Figure 4c and 4f; Table 1). The model however underestimates the depth of the upper-ocean stratification in the BoB during both seasons (Figures 4d and 4e).

[28] Longitudinal sections in the Bay (Figures 5a and 5b) and vertical profiles of climatological salinity and temperature north of 15°N (Figure 5c) further allow contrasting the thermohaline structure during premonsoon and postmonsoon seasons. Compared to premonsoon season, postmonsoon season displays much larger salinity stratification in the northern part of the Bay in the upper 40 m (∼0.1 psu m$^{-1}$ against ∼0.03 psu m$^{-1}$ before the monsoon). While the SST during the premonsoon season is higher than 29°C, the SST drops by ∼1°C during the postmonsoon season, explaining the deeper upper-ocean thermal stratification discussed on Figure 4. Once again, the model simulates the contrast between these two seasons reasonably well, both in terms of temperature and salinity stratification (Figures 5d, 5e, and 5f).

[29] Figure 6 shows the CI calculated from model and observations during premonsoon and postmonsoon seasons, as well as the difference between the two seasons. This measure also allows validating the relevant ocean stratification
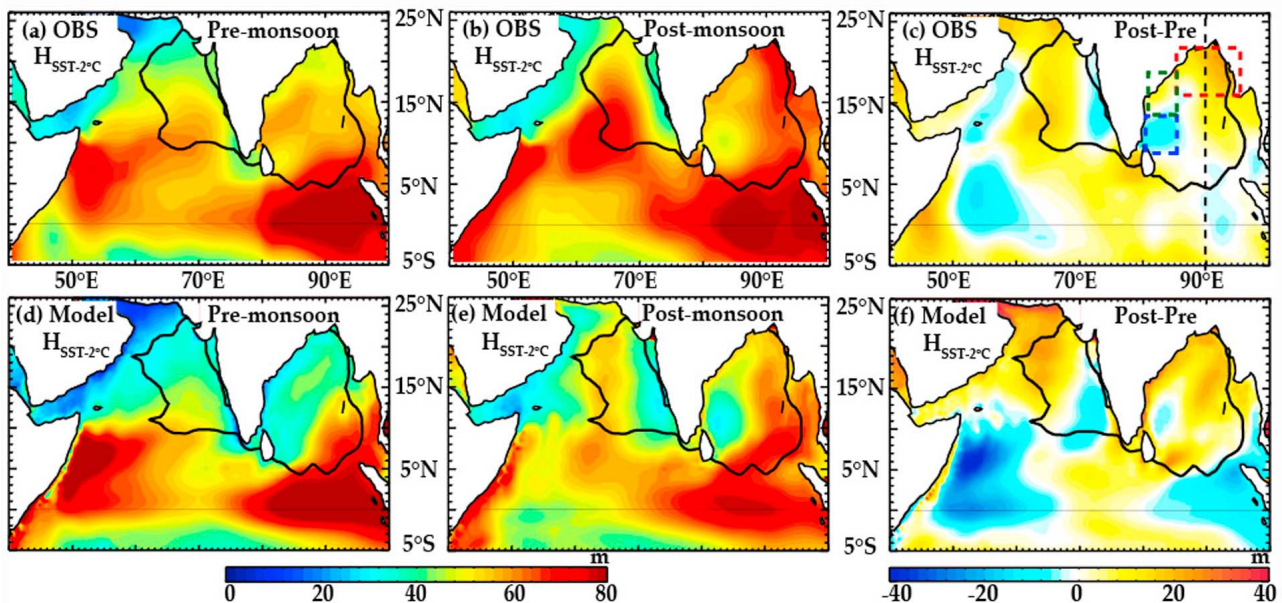


**Figure 4.** Climatological depth at which the ocean temperature is 2°C below the surface temperature (in meters) for (a and d) premonsoon and (b and e) postmonsoon seasons, and (c and f) their difference derived from (top) *de Boyer Montégut et al.* [2004] climatology and (bottom) the model over the 1978–2007 period. The thick contour delineates a region where 80% of TCs occur in the northern Indian Ocean (see Figure 1) while dashed colored boxes on Figure 4c are same as in Figure 3. The black dashed line indicates the temperature and salinity section at 90°E shown on Figure 5.
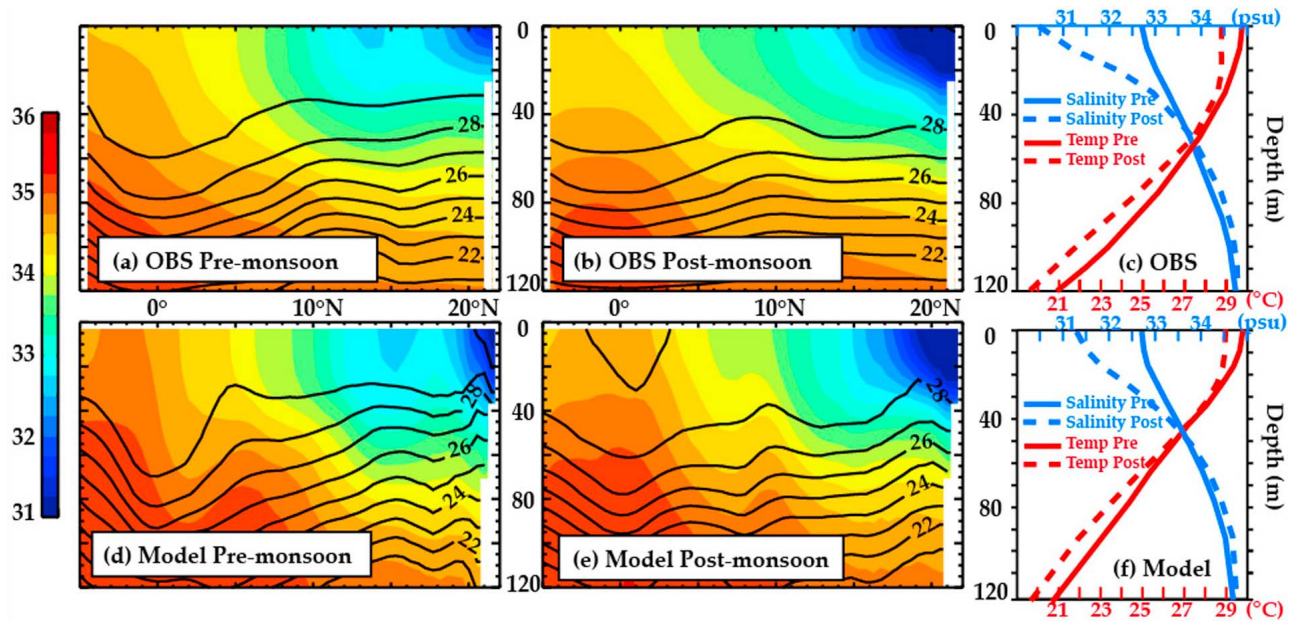
**Figure 5.** Latitude-depth section (at 90°E) of observed climatological salinity (in psu; color) and temperature (in °C; contour) in the BoB during (a) premonsoon and (b) postmonsoon seasons. (c) Observed temperature (red) and salinity (blue) profiles averaged in the BoB north of 15°N for premonsoon (plain line) and postmonsoon (dashed line) seasons. (d–f) Same for model outputs over 1978–2007.

for the response to TCs (V12b), which (contrary to $H_{SST-2°C}$) integrates the effect of salinity stratification. Observations indicate that the CI is relatively homogeneous during the premonsoon season in the Bay (Figure 6a), but displays a very strong northeast/southwest contrast during the postmonsoon season (Figure 6b). The northern and eastern part of the Bay as well as the eastern coast of India display the largest CI changes (Figure 6c and Table 1), corresponding to a ~20 to 30% CI increase (Figure 6). In contrast, the southwestern part of the Bay exhibits opposite seasonal changes, with a ~10% CI reduction offshore of Tamil Nadu and north of Sri Lanka. Seasonal CI changes estimated from model
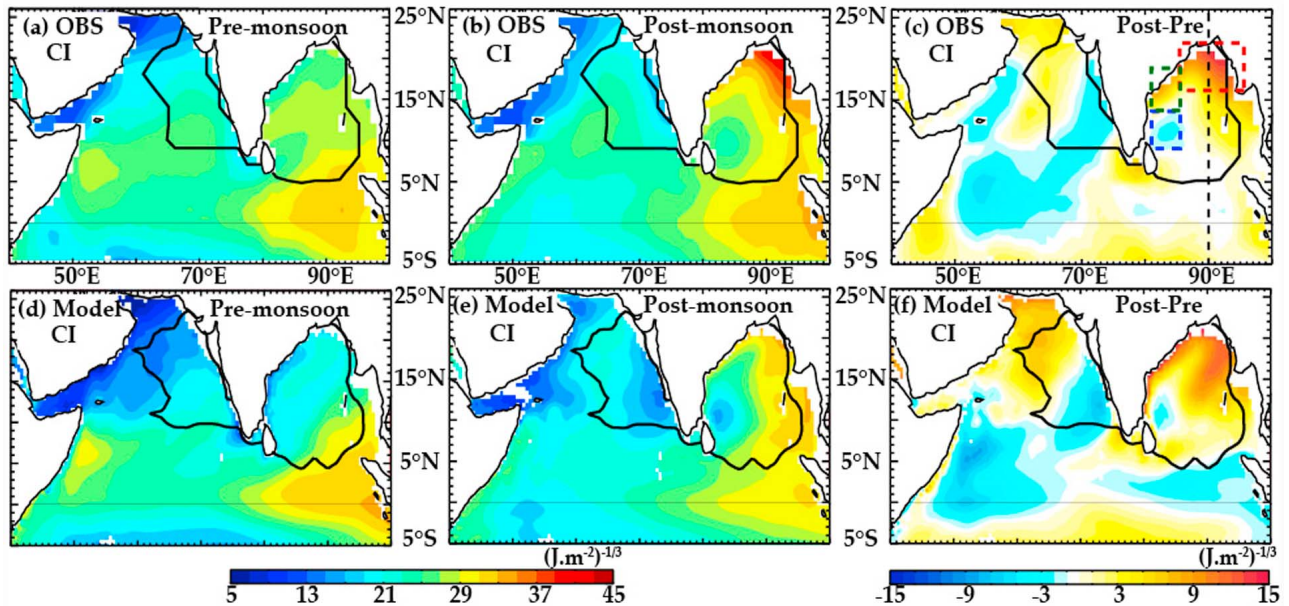


**Figure 6.** Climatological cooling inhibition index (CI; in $(J.m^{-2})^{-1/3}$) for (a and d) premonsoon and (b and e) postmonsoon seasons, and (c and f) their difference using (top) observations and (bottom) the model over the 1978–2007 period. The thick contour delineates a region where 80% of TCs occur in the northern Indian Ocean (see Figure 1) while dashed colored boxes on Figure 6c are same as in Figure 3. The black dashed line indicates the temperature and salinity section at 90°E shown on Figure 5.
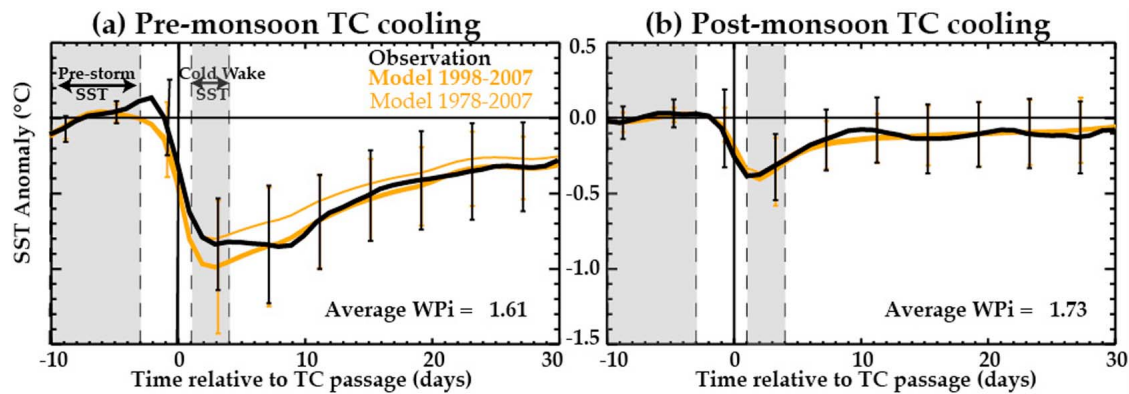
**Figure 7.** Composite evolution of TC-induced SST cooling within 200 km of TC-tracks in the BoB (in °C) during (a) premonsoon and (b) postmonsoon seasons for observations (black line) and the model over the 1998–2007 period (thick orange line) and the model over the 1978–2007 period (thin orange line). Vertical bars (black for the observations and orange for the model) indicate the spread around the mean, evaluated from the lower and upper quartiles. These quartiles are not shown for the model results over the 1978–2007 period for clarity.

outputs generally agree qualitatively with those inferred from the observed climatology (Figures 6c and 6f, Table 1). The physical meaning of this pattern follows: the deeper thermal stratification (Figures 4 and 5) resulting from the cooler SST and strong near surface salinity gradient in the northern part of the Bay (Figures 3 and 5) result in a stronger oceanic inhibition of vertical mixing-driven cooling during the postmonsoon season, compared to the premonsoon season. A given TC is hence likely to induce a weaker cooling during the postmonsoon season, especially in the northeastern part of the Bay and along the eastern Indian coastline. The model underestimates the CI in the BoB during both seasons (Figures 6d and 6e) but displays similar seasonal change (Figure 6f and Table 1).

[30] Figure 7 provides a first illustration of the potential impact of this seasonal change in stratification on TC-induced cooling. The composite TC-induced surface cooling amplitude derived from satellite observations over the 1998–2007 period is significantly larger during premonsoon (~0.9°C; Figure 7a) than during postmonsoon (~0.4°C; Figure 7b) season in the BoB. Largest cooling usually occurs ~2–3 days after the cyclone passage and recedes within ~20 days although the SST remains on average 0.1–0.4°C colder than prestorm SSTs, as previously discussed by *Lloyd and Vecchi* [2011]. The model accurately reproduces both the amplitude and timing of the TC induced SST cooling, before and after the monsoon, although with a slightly overestimated cooling (Figure 7). The above results agree well with previous observations underneath individual TCs in the BoB, with larger cooling during premonsoon season [*Gopalakrishna et al.*, 1993; *Rao*, 1987; *Sengupta et al.*, 2008] than during postmonsoon season [*Chinthalu et al.*, 2001; *Sengupta et al.*, 2008; *Subrahmanyam et al.*, 2005]. The mean wind power over the cyclone tracks does not differ much between the premonsoon and postmonsoon seasons (WPi: 1.61 against 1.73; Figure 7). The distribution of WPi for both seasons is further displayed on Figure 8c: the two distributions are very much alike with mean values (vertical lines) that are not significantly different at 95% level in the two cases. In contrast, the TC-induced cooling distributions are significantly

different with a weaker mean during the postmonsoon seasons and most intense observed cooling (up to −2.5°–3°C) occurring only during the premonsoon season for observations (Figure 8a). The modeled cooling exhibits a similar behavior (Figure 8b), although the mean for both seasons are overestimated by 10 to 20% as compared to observations. This overestimation is likely related to the underestimation of the climatological CI (see Figure 6). The weak differences in WPi (i.e., in TC mechanical energy transfer to the ocean) between the two seasons are a first indication that ocean stratification is the main responsible for differences in cooling amplitude.

## 4. Processes Controlling Differences in Premonsoon and Postmonsoon TC Cooling

[31] In the previous section, we only used model results from the satellite period (1998–2007) to allow a fair comparison with observations. The results discussed in the previous section remain true over the full 1978–2007 model simulation period: a weaker cooling is simulated during the postmonsoon compared to the premonsoon season over the 1978–2007 period (Figure 7), while the wind power remains very similar (not shown). In this section, we hence analyze the model response to 135 TCs in the BoB over the 1978–2007 period, in order to obtain a larger sample and a higher statistical significance.

[32] Figure 9 exhibits the histograms of TC-induced SST cooling as a function of WPi for the premonsoon and postmonsoon seasons. These two distributions are strikingly different: the slope of the average cooling amplitude against WPi is about three times smaller during the postmonsoon season than during the premonsoon season (0.28°C against 0.70°C). This result demonstrates that, for a given wind power input, the resulting cooling is on average two to three times smaller during the postmonsoon season. Differences in oceanic stratification underneath TCs between the two seasons are further demonstrated by displaying probability density functions of the CI (Figure 8d). The CI distribution is significantly different between the two seasons, with
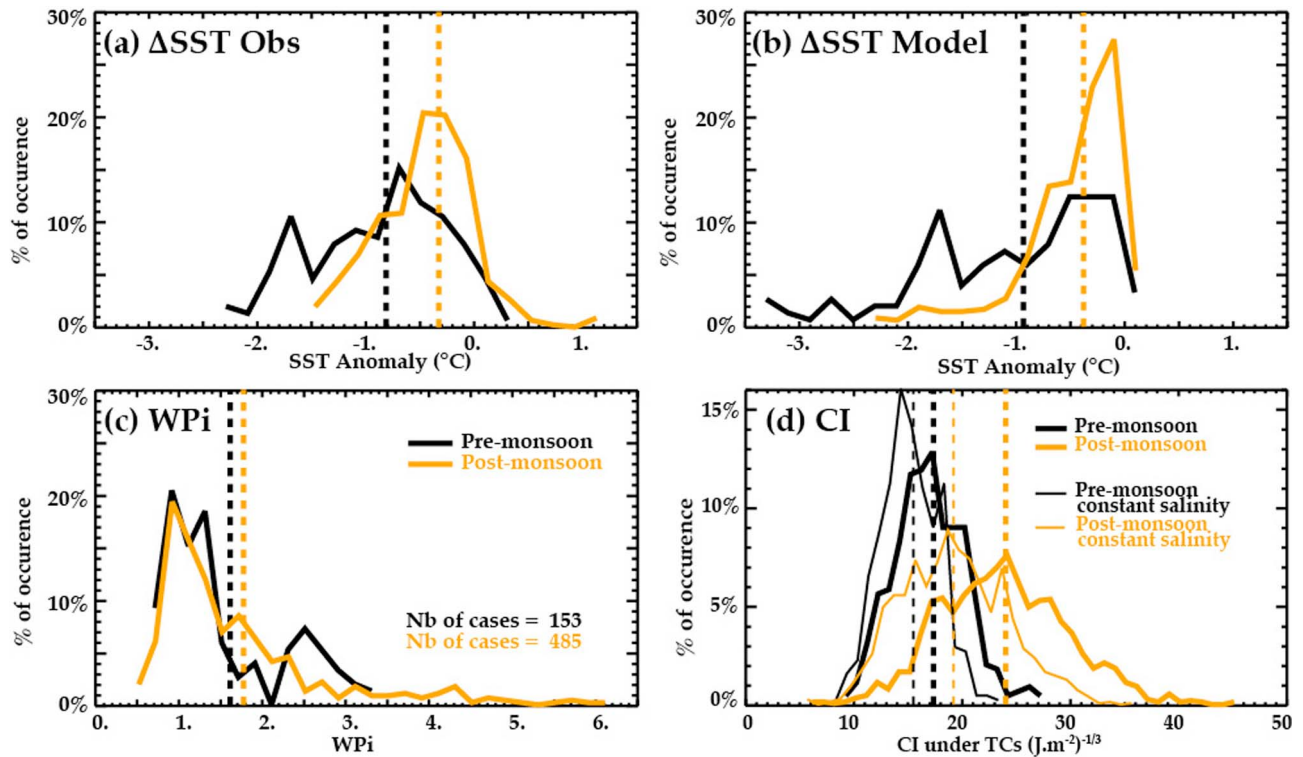
**Figure 8.** Probability density function in the BoB for pre-monsoon (black thick line) and post-monsoon seasons (orange thick line) of the TC-related distributions of (a) observed TC-induced SST cooling (bin size: 0.2°C), (b) modeled TC-induced SST cooling (bin size: 0.2°C), (c) WPi (bin size: 0.2), and (d) CI (bin size: 1) over the 1998–2007 period. The number of cases on Figure 8c represents the number of cooling locations, sampled every 6 h along the TC tracks. The thin black (orange) line on Figure 8d indicate the premonsoon (postmonsoon) CI calculated with a constant salinity profile ($CI_{S0}$) of 33.85 psu (averaged salinity in the BoB in postmonsoon season within the upper 200 m). Vertical thick dashed lines on each panel indicate the mean value for premonsoon (black) and postmonsoon season (orange). The vertical thin dashed lines on Figure 8d indicate the mean value for premonsoon (black) and postmonsoon (orange) $CI_{S0}$.

stronger near-surface haline stratification and deeper thermal stratification (i.e., stronger CI) during the postmonsoon season. The range of CI values under which TCs occur is also larger during postmonsoon than during premonsoon season. While CI values above 22 are hardly found underneath TCs before the monsoon, half of CI values exceed this threshold during the months following the monsoon. The influence of oceanic stratification on TC-induced cooling amplitude is further demonstrated by the colored curves on Figure 9 that display the average cooling as a function of WPi for four different ranges of CI (less than 18, between 18 and 24, between 24 and 30, and greater than 30). The influence of CI allows explaining the wide range of possible TC-induced cooling amplitudes for a given wind power input and hence the dispersion of TC-induced cooling during the postmonsoon season seen on Figure 9b. When TCs transit over waters displaying large CI (greater than 30, i.e., strongly stratified) during the postmonsoon season, the resulting cooling amplitudes are very weak (regression slope of 0.04°C). In contrast, cooling amplitudes for TCs that transit over waters with lowest CI (less than 18; i.e., weakly stratified) are larger (~0.74°C) and match those simulated during premonsoon season (slope of 0.74°C). This demonstrates that

oceanic stratification is a major factor controlling the amplitude of the SST response to a TC in the BoB.

[33] An analysis of the physical processes responsible for the simulated TC-induced cooling (Figure 10) derived from the online tendency terms of the equation of the ML temperature described in section 2.2 provides further evidence on the role of upper-ocean stratification in the cooling amplitude difference between the two seasons. TC cooling induced by heat fluxes (mainly latent; not shown) is indeed very similar between the two seasons and does not exceed −0.5°C for the strongest TC forcing (WPi > 2.5, compare the orange curves in Figures 10a and 10b). Advective processes are of secondary importance and only slightly contribute to TC-induced cooling for the strongest WPi (i.e., strongest cyclones). In contrast, the amplitude of mixing-induced cooling strongly differs between the two seasons. During premonsoon, mixing-induced cooling rapidly increases with WPi, explaining more than 60% of the TC-induced cooling for WPi larger than 1.5. In contrast, mixing-induced cooling is three to four times weaker during the postmonsoon season for a given wind power input and never exceeds the amplitude of the cooling induced by heat fluxes. This reduced cooling by vertical mixing is largely responsible for the reduced TC-induced cooling amplitude for the
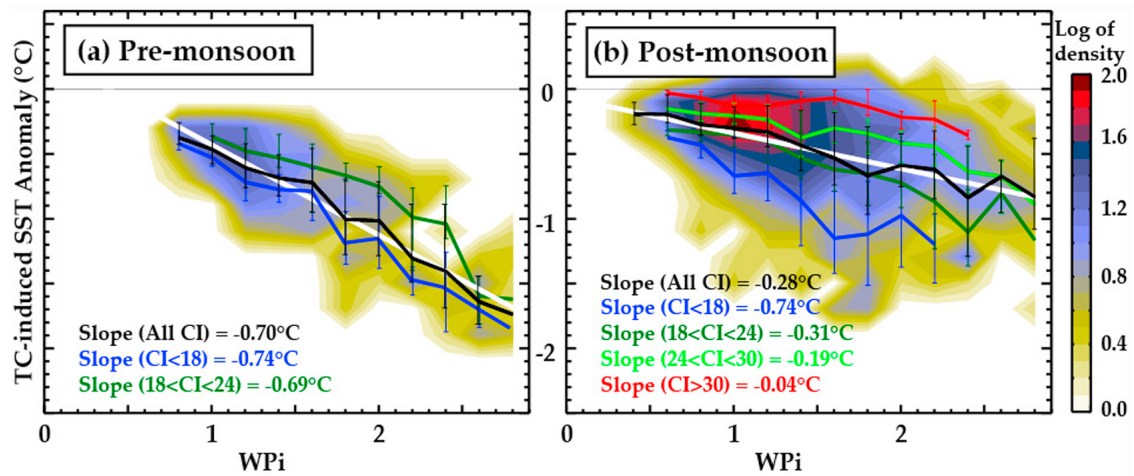
**Figure 9.** Two-dimensional histograms of TC-induced SST cooling (in °C) versus WPi in the model over the entire period (1978–2007) for (a) premonsoon and (b) postmonsoon seasons. The thick black line indicates the average of the cooling distribution for a given WPi, the white line is a linear fit of the black line, and the vertical black bars indicate the upper and lower quartiles of the cooling distribution for a given WPi. The slope of the linear fit is also reported on each panel. The average cooling (in °C) as a function of WPi for different CI (in $(J.m^{-2})^{-1/3}$) ranges (CI < 18, 18 < CI < 24, 24 < CI < 30, CI > 30) during premonsoon (Figure 9a) and postmonsoon (Figure 9b) seasons is indicated with colored lines. Results for the two upper CI ranges (24 < CI < 30 and CI > 30) are not displayed during premonsoon season due to the lack of oceanic profiles with such CIs at this time of the year. Vertical color bars indicate the upper and lower quartiles of the cooling distribution for a given WPi, for each range of CI. The slope of the linear fit of each curve is reported on each panel.

postmonsoon season compared to premonsoon season. This tendency term analysis demonstrates that cooling by mixing is weaker during the postmonsoon season. This is because the stronger upper-ocean stratification opposes a stronger resistance to mixing, hence resulting in a lesser entrainment of colder subsurface water. This is one more indication that changes in ocean stratification explain most differences in TC-induced cooling between the two seasons.

[34] The oceanic stratification depends on both temperature and salinity. Using the CI, it is possible to infer their respective contributions to the total stratification and relate them to TC-induced surface cooling differences between the two seasons. Figure 8d compares the distribution of the CI underneath TCs for the two seasons calculated with a constant salinity profile of 33.85 psu (the average upper 200 m BoB value in postmonsoon season; hereafter $CI_{S0}$; results are not very sensitive to the salinity value used to perform this calculation). This index therefore only accounts for thermal stratification effects. The overall $CI_{S0}$ distribution is shifted toward lower values compared to CI (Figure 8d); i.e.,
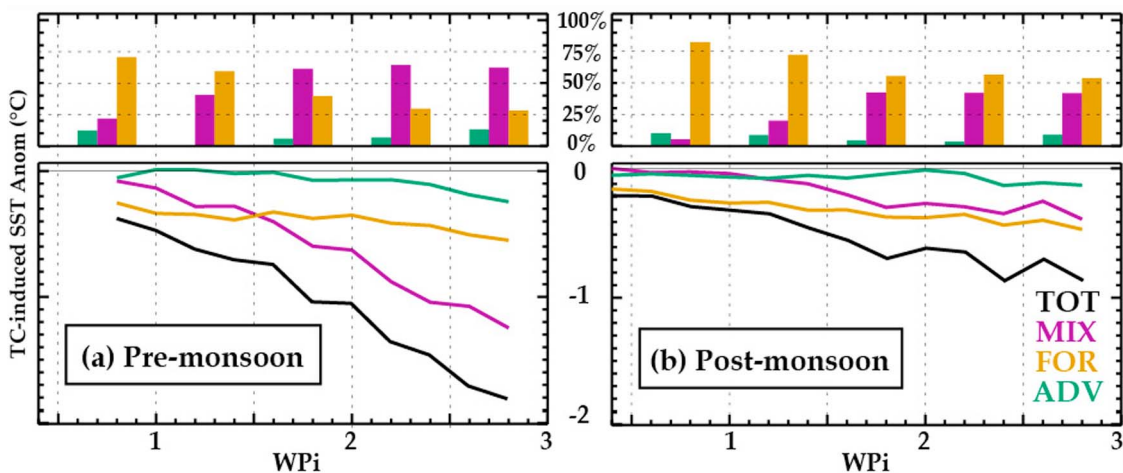


**Figure 10.** Mean amplitude of TC-induced cooling and respective contributions of vertical mixing (MIX), heat fluxes (FOR), and advection (ADV) to the total cooling as a function of the WPi for (a) premonsoon and (b) postmonsoon seasons. Absolute values (relative contribution of each process to the total cooling) of each process to the total cooling are shown on the bottom (top).
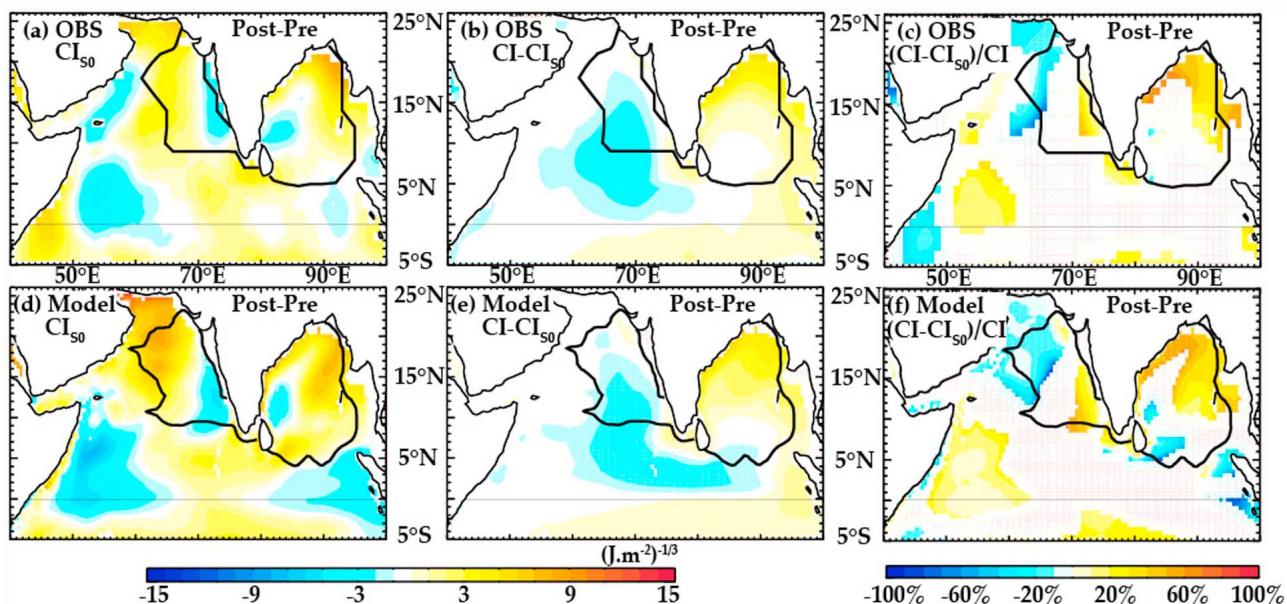
**Figure 11.** Postmonsoon minus premonsoon Cooling Inhibition index calculated with constant salinity profile $CI_{S0}$ (a and d), $CI-CI_{S0}$ (b and e), and percentage of CI seasonal change due to salinity $(CI-CI_{S0})/CI$ (c and f) using (top) observations and (bottom) model outputs. The middle column indicates the salinity propensity to inhibit cooling underneath TCs (i.e., the right column has yellow shading where salinity contributes to diminish TC-induced cooling during the postmonsoon season, relative to the premonsoon season). On the right is only displayed the salinity contribution for absolute CI seasonal changes larger than $2(J.m^{-2})^{-1/3}$.

salinity stratification inhibits vertical mixing in the BoB. This is an expected result as salinity strongly contributes to upper ocean static stability in the upper BoB (Figure 5). The impact of salinity on stratification is twice larger during the postmonsoon than during the premonsoon season in the BoB ($CI-CI_{S0} \sim 2$ on average during premonsoon season and $\sim 5$ during postmonsoon season). This simple diagnostic illustrates the key role of salinity in density stratification of the BoB, especially during the postmonsoon season.

[35] Figure 11 further illustrates the regional distribution of salinity impact on the BoB stratification (i.e., differences between CI and $CI_{S0}$). As displayed on Figure 11c, salinity seasonal changes mainly affect the CI distribution along the northern rim of the BoB, where strongest seasonal changes in haline stratification (Figures 3 and 5) and BLT (Figure 3) are observed. Salinity accounts for about half of the seasonal cooling inhibition changes in the northeastern part of the Bay along the coast of Myanmar and Bangladesh and for a large part of CI increase along the eastern coast of India, offshore the state of Andhra Pradesh. On the other hand, temperature changes explain all of CI seasonal changes in the southwestern part of the Bay (Figure 11a). The model generally reproduces these features (Figures 11d–11f), although it slightly underestimates the relative role of haline stratification in the CI changes along the eastern Indian coastline.

[36] While these results clearly demonstrate the important role played by salinity (ranging from less than 0% to more than 80% depending on the considered region), observational estimates and model results both indicate a strong contribution from the seasonal evolution of the thermal structure to the premonsoon and postmonsoon CI contrasts.

The deepening of the upper thermocline related to the seasonal surface cooling in the northern and western part of the BoB (Figures 4 and 5) acts to increase the CI in these regions during postmonsoon season (Figures 11a and 11d) and contributes up to 80% of the seasonal stratification changes (Figures 11c and 11f). Typically, because of the surface cooling taking place during the monsoon, vertical mixing has to penetrate deeper (down to $\sim 50$ m) during the postmonsoon season, as compared to the premonsoon season (down to $\sim 35$ m), in order to cool the mixed layer by 2°C (Figure 4). While salinity and temperature changes act in concert to increase CI after the monsoon along the northern rim of the BoB, they oppose each other in the southwestern part. The freshening acts to increase CI (Figure 3) while both the SST drop (Figure 5) and the modest shoaling of the thermal stratification (Figure 4) act to decrease CI in this latter region (Figure 11).

[37] Our results clearly indicate that seasonal changes in the vertical haline and thermal structures are consistent with differences in TC-induced cooling amplitude between the premonsoon and postmonsoon seasons. A more quantitative estimate of their respective roles can further be obtained by using the least squares fit of the cooling amplitude as a function of WPi and CI discussed in section 2.3 to hindcast the simulated cooling in the BoB. This approach performs very well, with a 0.84 correlation and a 0.98 regression between the amplitudes of the cooling simulated by the model and the cooling hindcasted using the least square fit (Figure 12). The histograms of the hindcasted SST cooling as a function of WPi (Figures 13a and 13b) also show a very similar behavior to the SST cooling actually simulated by
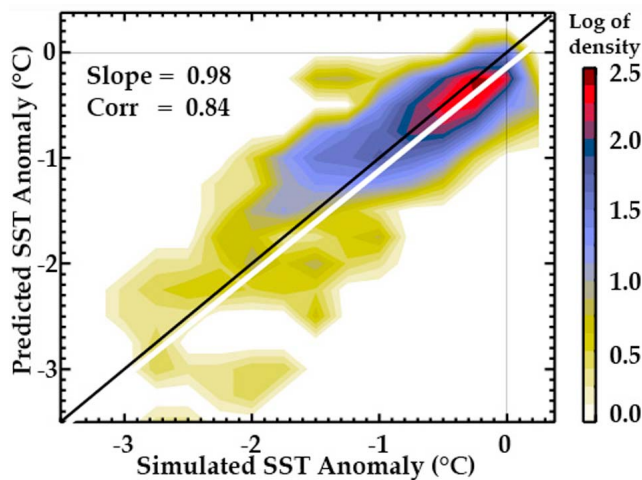
**Figure 12.** Two-dimensional histogram of predicted SST cooling versus simulated SST cooling in the BoB over the period 1978–2007. The regression slope and correlation between the two data sets are indicated. The black line corresponds to the y = x curve, and the white line corresponds to the best linear fit.

the model (Figure 9). The slope of the predicted cooling amplitude against WPi is indeed larger during the premonsoon season ($-0.62°C$, compared to $-0.70°C$ for the simulated cooling, Figure 9a) than during the postmonsoon season ($\sim -0.28°C$ for both predicted and simulated coolings). The influence of salinity on cooling amplitude can then be assessed from a cooling prediction using $CI_{S0}$. The cooling slope as a function of WPi only increases by $\sim 10\%$ when neglecting haline stratification for premonsoon season (Figures 13a and 13c). This suggests a relatively modest role of salinity on the amplitude of TC-induced cooling in the premonsoon season. In contrast, using $CI_{S0}$ for the postmonsoon period results in a 50% increase of the slope from $-0.28°C$ to $-0.41°C$ and hence in a $\sim 50\%$ increase of the hindcasted mean cooling amplitude (Figures 13b and 13d). In addition, the very weak predicted and simulated TC-induced coolings ($-0.3°C < SST < 0.0°C$) for moderate WPi ($1 < WPi < 2$) occur much less often when salinity is not accounted for. However, the change of slope due to haline stratification during the postmonsoon season (from $-0.28°C$ to $-0.41°C$; Figures 13b and 13d) only explains 40% of the change of slope between postmonsoon and premonsoon seasons (from $-0.28°C$ to $-0.62°C$; Figures 13a and 13b). This indicates that changes in haline stratification are responsible on average for $\sim 40\%$ of the cooling reduction between premonsoon and the postmonsoon seasons, with changes in the thermal stratification explaining the remaining 60%. In other words, salinity effects reduce TC-induced cooling by 40% during the postmonsoon season.

# 5. Summary and Discussion

## 5.1. Summary

[38] In this paper, we investigate processes responsible for the smaller amplitude TC-induced surface cooling in the BoB during the postmonsoon compared to the premonsoon

season. Because detailed observations underneath TCs are scarce, we analyze a global ocean model simulation forced by realistic TC winds derived from an analytic shape adjusted to observed TC tracks and magnitude over the 1978–2007 period. Our approach samples the ocean response to 135 TCs in the BoB over this 30-year period. The model exhibits TC-induced SST cooling that is about 3 times larger during the premonsoon than during postmonsoon season, in agreement with observations.

[39] As discussed by V12b, the amplitude of TC cooling is to a large extent explained by two parameters: the wind power input of the TC atmospheric forcing and the cooling inhibition from background oceanic conditions. TC wind power input does not significantly change between the premonsoon and postmonsoon seasons, suggesting that seasonal changes in oceanic structure are responsible for larger TC-induced cooling amplitude during premonsoon season. The heavy precipitation and river discharge during and following the monsoon result in a very intense upper-ocean freshening and the formation of a thick BL. Thermal structure also undergoes marked changes between premonsoon and postmonsoon seasons, with a cooler mixed layer over most of the BoB following the monsoon, resulting in a deeper upper thermal stratification. These thermal and haline stratification changes reduce the entrainment of cooler thermocline waters into the mixed layer and consequently reduce TC-induced cooling during the postmonsoon season. Our analysis indeed reveals that stronger cooling inhibition by oceanic stratification is responsible for a cooling amplitude reduction by a factor of three during the postmonsoon season.

[40] We then assess the respective contributions of seasonal changes in thermal and haline stratification to the reduction of TC-induced cooling. To that end, we use a simple bivariate statistical model that allows accurately predicting the amplitude of TC-induced cooling from wind power (WPi) and CI indices. This allows demonstrating that the strong near-surface salinity stratification during the postmonsoon season is responsible for $\sim 40\%$ of cooling decrease, with SST changes explaining the remaining 60%. The respective contributions of thermal and haline stratification however strongly vary spatially within the Bay: haline stratification explains most of the TC-induced cooling inhibition offshore of the eastern coast of India ($\sim 80\%$), where salinity seasonal changes are strongest while thermal stratification explains all the TC-induced cooling inhibition in the southwestern part of the BoB.

## 5.2. Discussion

[41] Our modeling study confirms previous case studies. Observations indeed suggest that TC-induced surface cooling is larger during the premonsoon [*Gopalakrishna et al.*, 1993; *Rao*, 1987; *Sengupta et al.*, 2008] than during the postmonsoon season in the BoB [*Chinthalu et al.*, 2001; *Sengupta et al.*, 2008; *Subrahmanyam et al.*, 2005]. *Sengupta et al.* [2008] suggest that weaker surface cooling during the postmonsoon season largely results from the presence of salinity and BL changes through individual case studies analysis. Our results, however, suggest that thermal changes are a major contributor to the difference in TC-induced cooling amplitude between the two seasons, although the
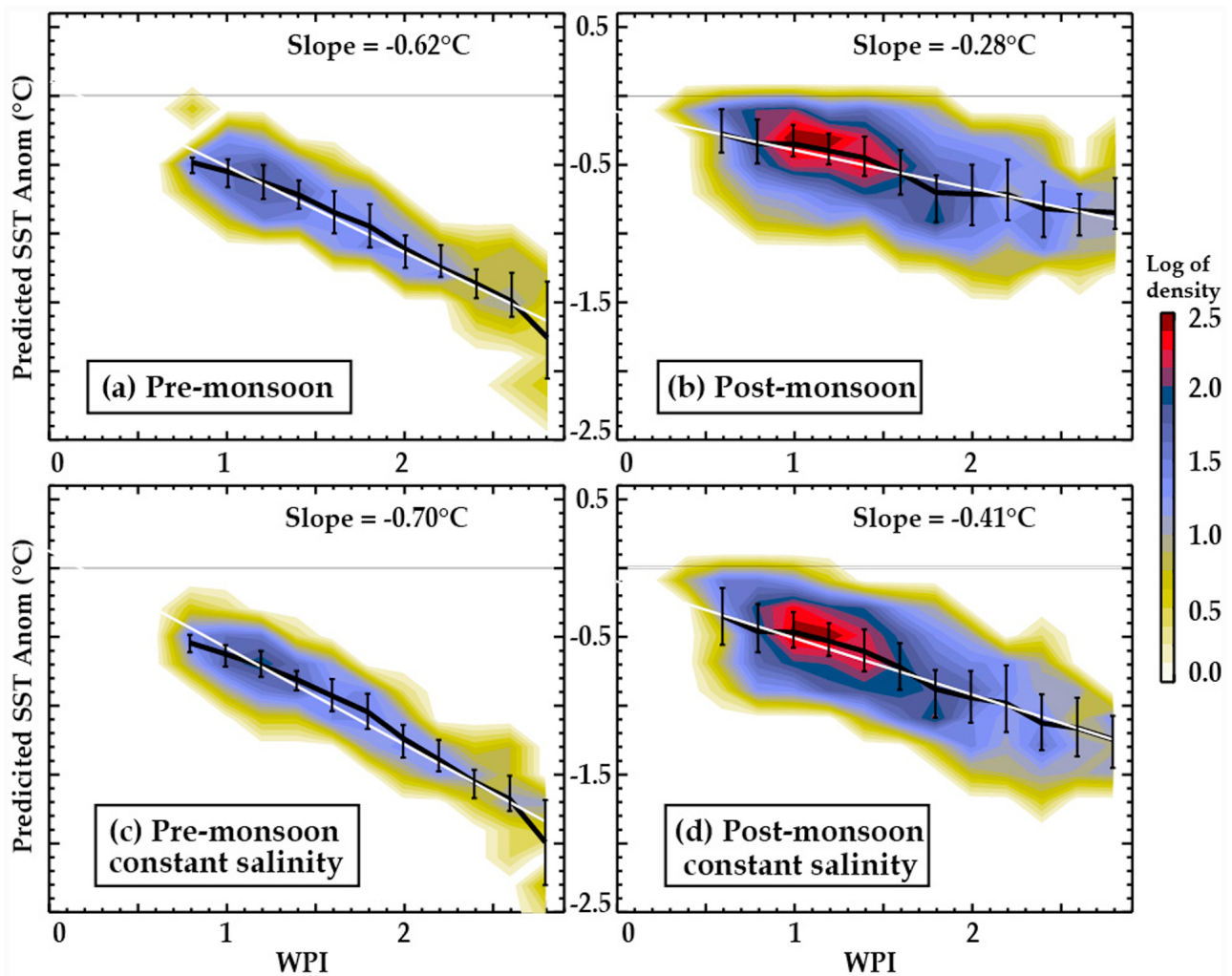
**Figure 13.** Two-dimensional histograms of predicted SST cooling with (a and b) actual T, S profiles and with (c and d) a constant salinity profile versus WPi during (left) premonsoon and (right) postmonsoon seasons in the BoB. The thick black line indicates the average of the cooling distribution for a given WPi, the vertical bars indicate the upper and lower quartiles of the cooling distribution for a given WPi, and the white line is a linear fit of the black line. The slope of the linear fit is reported as a white line.

effects of the changes in haline stratification also significantly contribute the seasonal TC-induced cooling changes, especially around the rim of the northern BoB.

[42] Satellite observations show that the amplitude of TC-induced surface cooling is also larger during the premonsoon (~1.2°C) than during postmonsoon (~0.6°C) season in the Arabian Sea (Figures 14a and 14b). Our model simulation (38 Arabian Sea TCs over the 1978–2007 period) reproduces these premonsoon/postmonsoon TC-induced surface cooling contrasts in the Arabian Sea (Figures 14a and 14b). Figures 14c and 14d shows the histograms of TC-induced cooling as a function of WPi for premonsoon and postmonsoon seasons for the Arabian Sea. Unlike the BoB, there is a stronger wind power input before the monsoon than after (average WPi of ~2.5 against ~1.6). Compared to the Bay of Bengal, the regression slope of the TC-induced cooling to WPi does not considerably change between the premonsoon and postmonsoon seasons in the Arabian Sea (0.87°C/0.74°C, against 0.70°C/0.28°C in the

BoB) and is close to the 0.70°C slope during premonsoon season in the BoB. The stronger cooling during premonsoon season hence largely results from changes in TC wind power input. Owing to a less salinity-stratified upper ocean [e.g., *Shenoi et al.*, 2002], the CI is lower in the Arabian Sea than in the BoB (Figure 6). During the postmonsoon season, salinity stratification acts to decrease the CI in the central part of the Arabian Sea (Figures 11b and 11e) due to lower salinity at depth (not shown). This hence partly compensates the CI increase due to changes in the thermal structure west of 70°E (Figures 11a and 11d), resulting in a relatively small influence of the oceanic stratification on the cooling in the Arabian Sea, compared to the BoB.

[43] The rather coarse resolution model used in the present study simulates rather accurately the contrasted TC-induced cooling amplitude between premonsoon and postmonsoon seasons, suggesting that the 1/2° resolution is sufficient to capture the TC-induced mixing, a dominant process in the cold wake formation. Refined resolution in the BoB within
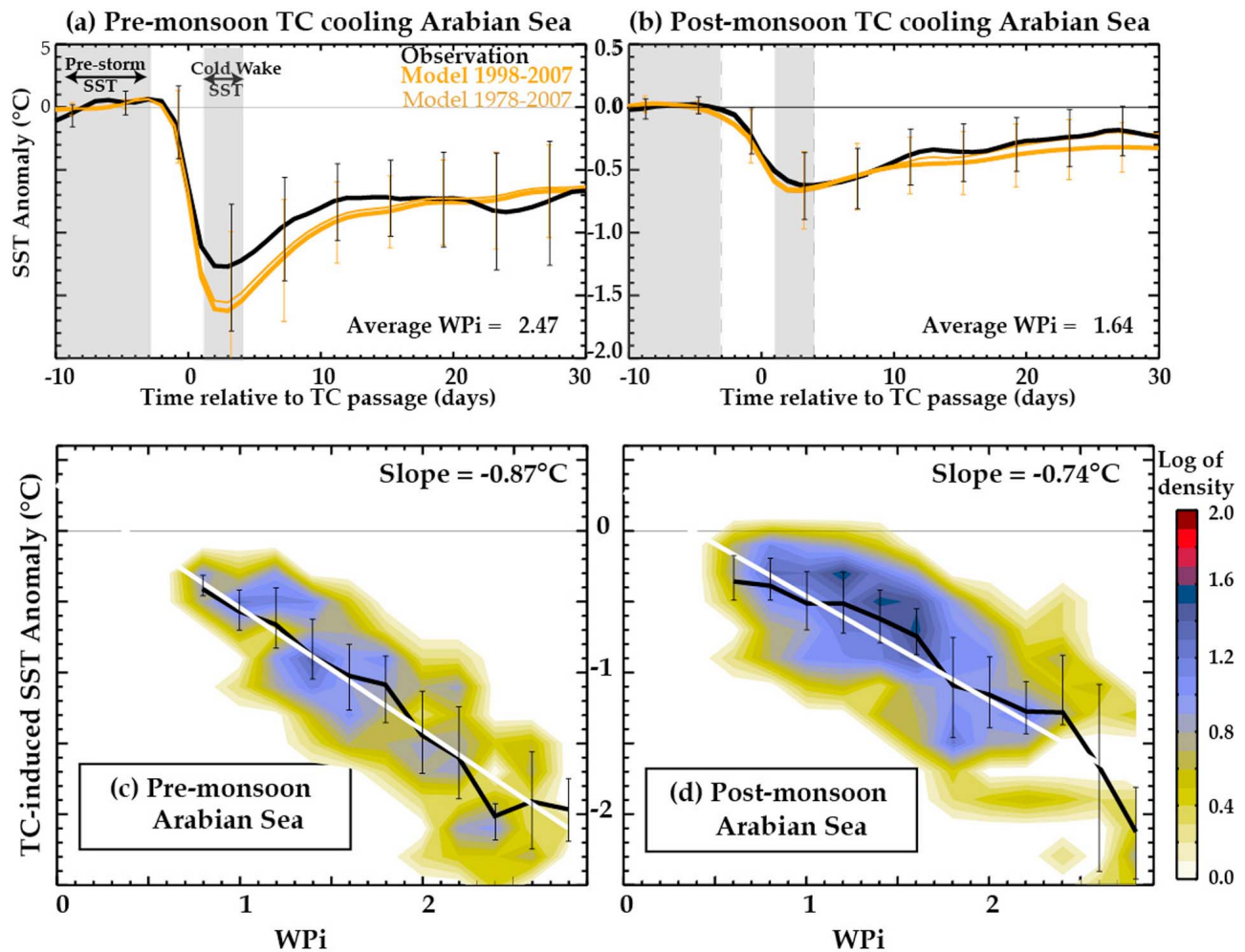
**Figure 14.** (a and b) Same as Figure 7a and 7b but for the Arabian Sea. (c and d) Same as Figure 9 (but without the binning into CI), for the Arabian Sea.

our global model [*Biastoch et al.*, 2008b] or the use of high-resolution regional models [*Diansky et al.*, 2006; R. Benshila et al., The upper Bay of Bengal salinity structure in a high-resolution model, submitted to *Ocean Modelling*, 2012] may however be required to better represent the TC-induced Ekman suction that shoals the thermocline near the eye, increasing the cooling efficiency of vertical mixing [*Yablonsky and Ginis*, 2009; *Jullien et al.*, 2012]. Although presumably of secondary importance [*Jacob and Koblinsky*, 2007; *Jourdain et al.*, 2012], a realistic parametrization of the TCs-related precipitation may as well improve the TC-induced ocean response, by accounting for their stabilizing effect on the water column. As shown by *Jourdain et al.* [2012], this stabilizing effect may reduce the cooling amplitude by 5 to 10% in the Bay, hence reducing the model TC-induced cooling overestimation (Figure 7).

[44] A significant increase in the horizontal and vertical model resolutions together with an improved representation of river discharge and precipitation patterns within the Bay [*Papa et al.*, 2010] may also allow a better representation of the mixed layer and of the offshore export of coastal freshwaters. The model underestimation of the freshening in the northern BoB during the postmonsoon season indeed

probably results in an underestimation of the salinity influence on the TC-induced surface cooling. Estimates derived from the observed climatology however suggest that at least 50% of the reduction in TC-induced cooling amplitude may be related to thermal changes (Figure 11). The exact quantification of the influence of salinity may require a more exhaustive and in-depth analysis of oceanic controls on TC-induced cooling within the Bay using observations. The Argo program [*Gould et al.*, 2004] provides a unique opportunity to investigate this issue: started in 2002, this program has reached its targeted density in late 2006. The availability of both temperature and salinity profiles in the upper ocean with reasonable temporal and spatial coverage may allow quantifying the respective contributions of salinity and temperature stratifications on TC-induced cooling inhibition from in situ observations over the recent period.

[45] This influence of salinity on TC-induced cooling calls for a better description and understanding of salinity variations within the Bay. Previous studies have already shown that the seasonal salinity evolution is largely determined by the fresh water sources/sinks and the redistribution of the resulting low/high-salinity water by ocean currents [e.g., *Rao and Sivakumar*, 2003; *Vinayachandran et al.*, 2005;
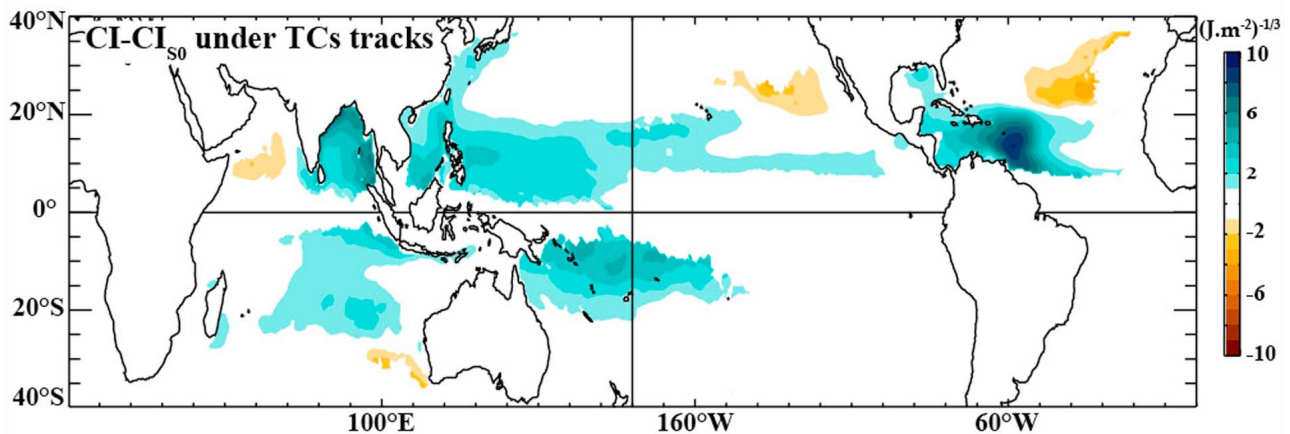
**Figure 15.** Spatial distribution of the difference between average standard CI underneath TC tracks (in $(J.m^{-2})^{-1/3}$) minus $CI_{S0}$ calculated over the 1978–2007 period. Both quantities are estimated from the weekly averaged stratification model outputs, within 200 km and between 10 days and 3 days before each cyclone eye passage location. This plot indicates where salinity stratification inhibits (blue shades) or enhances (red shades) TC-induced cooling.

*Sengupta et al.*, 2006]. However, the paucity of observations in coastal regions does not yet allow providing a robust and precise estimate of the intensity and extent of the BoB freshening. In addition, little is known about the interannual variability of SSS in the BoB. Although a limited amount of repeated observations along shipping lanes suggest that salinity variability is high in the tropical Indian Ocean [*Delcroix et al.*, 2005; *Rao and Sivakumar*, 2003], details of basin-wide spatiotemporal structure of salinity interannual variations in the BoB and their mechanisms are still lacking.

[46] This major influence of salinity also advocates for the use of an adequate oceanic index in statistical TC intensity prediction schemes. As shown by *Yu and McPhaden* [2011], buoyancy content in the BoB upper layer has a higher correlation with salinity content than with heat content. A commonly used metric of TC sensitivity to the ocean is the Tropical Cyclone Heat Potential (TCHP), a measure of the heat content between the sea surface and the depth of the 26°C isotherm, computed from altimeter-derived vertical temperature profile estimates [*Shay et al.*, 2000; *Goni and Trinanes*, 2003]. This index is useful for identifying warm anticyclonic features, where hurricanes often undergo sudden intensification in the western Atlantic [e.g., *Shay et al.*, 2000] and Northwestern Pacific [e.g., *Lin et al.*, 2005]. Using TCHP allows improving statistical intensity forecasts in these regions [*DeMaria et al.*, 2005; *Mainelli et al.*, 2008], where sea level variability is closely related to changes in the depth of the main thermocline, and salinity plays a lesser role. The present study advocates for the use of a different TC oceanic metric that accounts for the effect of salinity, as already suggested by V12b and *Yu and McPhaden* [2011]. The CI proposed by V12b is a relevant option, since it accounts for the effect of salinity stratification on TC-induced cooling inhibition. This metric can be derived from currently available operational oceanography products constrained by oceanic observations [e.g., *Drévillon et al.*, 2008] or directly from Argo data and tested in cyclone intensity forecast schemes in place of the currently used TCHP, in particular in the BoB.

[47] The present study brings further evidence of the haline stratification impact on TC-induced surface cooling. Neglecting haline stratification indeed results in a 50% overestimation of the TC-induced cooling during the postmonsoon season in the BoB (Figures 13b and 13d). Figure 15 shows the spatial distribution of the long-term average impact of salinity stratification on the precyclone cooling inhibition. Figure 15 hence provides a global view of regions where salinity stratification may significantly influence TC-induced SST cooling. Since TCs mostly develop in deep atmospheric convection regions, the associated climatological rainfall results in a stable haline stratification that inhibits TC-induced cooling, explaining the dominance of negative values in Figure 15. While the BoB, studied in this paper, is associated with a rather strong influence of haline stratification on TC-induced cooling, there is also a moderate influence of haline stratification in the western Pacific and South Indian Ocean TC basins. But there is a very clear influence of haline stratification on TC-induced cooling in the low-salinity region of the tropical western North Atlantic due to the discharge from the Amazon and Orinoco rivers whose waters are advected northwestward by the North Brazilian and Guyana Currents [*Muller-Karger et al.*, 1995; *Hellweger and Gordon*, 2002]. Given that TC that transit over this area can hit densely populated regions of Mexico and southeastern United States [*Weinkle et al.*, 2012], this region probably deserves a dedicated study.

[48] The haline stratification during the postmonsoon season induces an average 40% reduction of TC-induced cooling and potentially much more locally in the northern and eastern rim of the Bay. Given the potentially strong negative feedback of TC-induced cooling on TC intensity, an assessment of the exact impact of haline stratification on TC characteristics is however lacking. Further studies using high-resolution regional coupled models in this region as well as statistical analysis based on observations are therefore required to further address this issue, in the BoB and in the region influenced by the Amazon River plume.

# References

Alam, M. M., M. A. Hossain, and S. Shafee (2003), Frequency of Bay of Bengal cyclonic storms and depressions crossing different coastal zones, *Int. J. Climatol.*, 23, 1119–1125, doi:10.1002/joc.927.

Ali, M. M., C. M. Kishtawal, and J. Sarika (2007), Predicting cyclone tracks in the north Indian Ocean: An artificial neural network approach, *Geophys. Res. Lett.*, 34, L04603, doi:10.1029/2006GL028353.

Antonov, J. I., R. A. Locarnini, T. P. Boyer, A. V. Mishonov, and H. E. Garcia (2006), *World Ocean Atlas 2005, Volume 2: Salinity*, edited by S. Levitus, 182 pp., U.S. Govt. Print. Off., Washington, D.C.

Antonov, J. I., D. Seidov, T. P. Boyer, R. A. Locarnini, A. V. Mishonov, H. E. Garcia, O. K. Baranova, M. M. Zweng, and D. R. Johnson (2010), *World Ocean Atlas 2009, Volume 2: Salinity*, edited by S. Levitus, 184 pp., U.S. Govt. Print. Off., Washington, D.C.

Axell, L. B. (2002), Wind-driven internal waves and langmuir circulations in a numerical ocean model of the southern baltic sea, *J. Geophys. Res.*, 107(C11), 3204, doi:10.1029/2001JC000922.

Biastoch, A., C. W. Boning, J. Getzlaff, J.-M. Molines, and G. Madec (2008a), Causes of interannual-decadal variability in the meridional overturning circulation of the midlatitude North Atlantic ocean, *J. Clim.*, 21, 6599–6615, doi:10.1175/2008JCLI2404.1.

Biastoch, A., C. W. Boning, J. Lutjeharms, and M. Scheinert (2008b), Mesoscale perturbations control inter-ocean exchange south of Africa, *Geophys. Res. Lett.*, 35, L20602, doi:10.1029/2008GL035132.

Blanke, B., and P. Delecluse (1993), Variability of the tropical Atlantic ocean simulated by a general circulation model with two different mixed layer physics, *J. Phys. Oceanogr.*, 23, 1363–1388, doi:10.1175/1520-0485(1993)023<1363:VOTTAO>2.0.CO;2.

Burchard, H. (2002), Energy-conserving discretisation of turbulent shear and buoyancy production, *Ocean Modell.*, 4, 347–361, doi:10.1016/S1463-5003(02)00009-4.

Chatterjee, A., D. Shankar, S. S. C. Shenoi, G. V. Reddy, G. S. Michael, M. Ravichandran, V. V. Gopalkrishna, E. P. Rama Rao, T. V. S. Udaya Bhaskar, and V. N. Sanjeevan (2012), A new atlas of temperature and salinity for the north Indian Ocean, *J. Earth Syst. Sci.*, 121(3), 559–593, doi:10.1007/s12040-012-0191-9.

Chinthalu, G. R., P. Seetaramayya, M. Ravindran, and P. N. Mahajan (2001), Response of the Bay of Bengal to Gopalpur and Paradip super cyclones during 15–31 October, 1999, *Curr. Sci.*, 81, 283–291.

Cione, J. J., and E. W. Uhlhorn (2003), Sea surface temperature variability in hurricanes: Implications with respect to intensity change, *Mon. Weather Rev.*, 131, 1783–1796, doi:10.1175//2562.1.

Cione, J. J., P. G. Black, and S. H. Houston (2000), Surface observations in the hurricane environment, *Mon. Weather Rev.*, 128, 1550–1561, doi:10.1175/1520-0493(2000)128<1550:SOITHE>2.0.CO;2.

D'Asaro, E. A. (2003), The ocean boundary layer below Hurricane Dennis, *J. Phys. Oceanogr.*, 33, 561–579, doi:10.1175/1520-0485(2003)033<0561:TOBLBH>2.0.CO;2.

de Boyer Montégut, C., G. Madec, A. S. Fischer, A. Lazar, and D. Iudicone (2004), Mixed layer depth over the global ocean: An examination of profile data and a profile-based climatology, *J. Geophys. Res.*, 109, C12003, doi:10.1029/2004JC002378.

de Boyer Montégut, C., J. Vialard, S. S. C. Shenoi, D. Shankar, F. Durand, C. Ethé, and G. Madec (2007a), Simulated seasonal and interannual variability of the mixed layer heat budget in the northern Indian ocean, *J. Clim.*, 20, 3249–3268, doi:10.1175/JCLI4148.1.

de Boyer Montégut, C., J. Mignot, A. Lazar, and S. Cravatte (2007b), Control of salinity on the mixed layer depth in the world ocean. Part I: General description, *J. Geophys. Res.*, 112, C06011, doi:10.1029/2006JC003953.

Delcroix, T., A. Dessier, Y. Gouriou, and M. McPhaden (2005), Time and space scales for sea surface salinity in the tropical oceans, *Deep Sea Res.*, 52, 787–813, doi:10.1016/j.dsr.2004.11.012.

DeMaria, M., M. Mainelli, L. K. Shay, J. A. Knaff, and J. Kaplan (2005), Further improvements in the Statistical Hurricane Intensity Prediction Scheme (SHIPS), *Weather Forecast.*, 20, 531–543, doi:10.1175/WAF862.1.

Diansky, N. A., V. B. Zalesny, S. N. Moshonkin, and A. S. Rusakov (2006), High resolution modeling of the monsoon circulation in the Indian Ocean, *Oceanology, Engl. Transl.*, 46, 608–628.

Drévillon, M., et al. (2008), The GODAE/Mercator-Ocean global ocean forecasting system: Results, applications and prospects, *J. Operational Oceanogr.*, 1, 51–57.

Durand, F., D. Shankar, C. de Boyer Montégut, S. S. C. Shenoi, B. Blanke, and G. Madec (2007), Modeling the barrier-layer formation in the South-Eastern Arabian Sea, *J. Clim.*, 20, 2109–2120, doi:10.1175/JCLI4112.1.

Emanuel, K. A. (1999), Thermodynamic control of hurricane intensity, *Nature*, 401, 665–669, doi:10.1038/44326.

Emanuel, K. A. (2005), Increasing destructiveness of tropical cyclones over the past 30 years, *Nature*, 436, 686–688, doi:10.1038/nature03906.

Fekete, B. M., C. J. Vörösmarty, and W. Grabs (2002), High-resolution fields of global runoff combining observed river discharge and simulated water balances, *Global Biogeochem. Cycles*, 16(3), 1042, doi:10.1029/1999GB001254.

Goni, G. J., and J. A. Trinanes (2003), Ocean thermal structure monitoring could aid in the intensity forecast of tropical cyclones, *Eos Trans. AGU*, 84, 573–580, doi:10.1029/2003EO510001.

Gopalakrishna, V. V., V. S. N. Murty, M. S. S. Sarma, and J. S. Sastry (1993), Thermal response of upper layers of Bay of Bengal to forcing of a severe cyclonic storm: A case study, *Indian J. Mar. Sci.*, 22, 8–11.

Gopalan, A. K. S., V. V. Gopalakrishna, M. M. Ali, and R. Sharma (2000), Detection of Bay of Bengal eddies from TOPEX and in situ observations, *J. Mar. Res.*, 58, 721–734, doi:10.1357/002224000321358873.

Gould, J., et al. (2004), Argo profiling floats bring new era of in situ ocean observations, *Eos Trans. AGU*, 85, 185, doi:10.1029/2004EO190002.

Griffies, S., et al. (2009), Coordinated ocean-ice reference experiments (COREs), *Ocean Modell.*, 26, 1–46, doi:10.1016/j.ocemod.2008.08.007.

Han, W., and J. P. McCreary (2001), Modeling salinity distributions in the Indian Ocean, *J. Geophys. Res.*, 106, 859–877, doi:10.1029/2000JC000316.

Harenduprakash, L. L., and A. K. Mitra (1988), Vertical turbulent mass flux below the sea surface and air-sea interaction: Monsoon region of the Indian ocean, *Deep Sea Res.*, 43(8), 1423–1451.

Hellweger, F. L., and A. L. Gordon (2002), Tracing Amazon River water into the Caribbean Sea, *J. Mar. Res.*, 60, 537–549, doi:10.1357/002224002762324202.

Jacob, S., and C. Koblinsky (2007), Effects of precipitation on the upper-ocean response to a hurricane, *Mon. Weather Rev.*, 135, 2207–2225, doi:10.1175/MWR3366.1.

Jacob, S. D., and L. K. Shay (2003), The role of oceanic mesoscale features on the tropical cyclone-induced mixed layer response: A case study, *J. Phys. Oceanogr.*, 33, 649–676, doi:10.1175/1520-0485(2003)33<649:TROOMF>2.0.CO;2.

Jourdain, N., M. Lengaigne, J. Vialard, G. Madec, C. Menkes, E. Vincent, S. Jullien, and B. Barnier (2012), Observation based estimates of surface cooling inhibition by heavy rainfall under tropical cyclones, *J. Phys. Oceanogr.*, doi:10.1175/JPO-D-12-085.1, in press.

Jullien, S., C. E. Menkes, P. Marchesiello, N. C. Jourdain, M. Lengaigne, A. Koch-Larrouy, J. Lefèvre, E. M. Vincent, and V. Faure (2012), Impact of tropical cyclones on the heat budget of the South Pacific Ocean. *J. Phys. Oceanogr.*, 42, 1882–1906, doi:10.1175/JPO-D-11-0133.1.

Keerthi, M. G., M. Lengaigne, J. Vialard, C. de Boyer Montegut, and P. M. Muraleedharan (2012), Interannual variability of the Tropical Indian Ocean mixed layer depth, *Clim. Dyn.*, doi:10.1007/s00382-012-1295-2, in press.

Kikuchi, K., B. Wang, and H. Fudeyasu (2009), Genesis of tropical cyclone Nargis revealed by multiple satellite observations, *Geophys. Res. Lett.*, 36, L06811, doi:10.1029/2009GL037296.

Knapp, K. R., M. C. Kruk, D. H. Levinson, H. J. Diamond, and C. J. Neumann (2010), The International Best Track Archive for Climate Stewardship (IBTrACS): Unifying Tropical Cyclone Data, *Bull. Am. Meteorol. Soc.*, 10, 363–376, doi:10.1175/2009BAMS2755.1.

Kurian, J., and P. N. Vinayachandran (2007), Mechanisms of formation of Arabian Sea mini warm pool in a high resolution OGCM, *J. Geophys. Res.*, 112, C05009, doi:10.1029/2006JC003631.

Large, W., and S. Yeager (2009), The global climatology of an interannually varying air–sea flux data set, *Clim. Dyn.*, 33, 341–364, doi:10.1007/s00382-008-0441-3.

Leipper, D. F. (1967), Observed Ocean Conditions and Hurricane Hilda, 1964, *J. Atmos. Sci.*, 24, 182–186, doi:10.1175/1520-0469(1967)024<0182:OOCAHH>2.0.CO;2.

Lengaigne, M., U. Hausmann, G. Madec, C. Menkes, J. Vialard, and J. M. Molines (2012), Mechanisms controlling warm water volume interannual variations in the equatorial Pacific: Diabatic versus adiabatic processes, *Clim. Dyn.*, 38, 1031–1046, doi:10.1007/s00382-011-1051-z.

Lin, I. I., C. C. Wu, K. A. Emanuel, I. H. Lee, C. R. Wu, and I. F. Pun (2005), The interaction of Supertyphoon Maemi (2003) with a warm ocean eddy, *Mon. Weather Rev.*, *133*, 2635–2649, doi:10.1175/MWR3005.1.

Lloyd, I. D., and G. A. Vecchi (2011), Observational evidence of oceanic controls on hurricane intensity, *J. Clim.*, *24*, 1138–1153, doi:10.1175/2010JCLI3763.1.

Locarnini, R. A., A. V. Mishonov, J. I. Antonov, T. P. Boyer, and H. E. Garcia (2006), *World Ocean Atlas 2005, Volume 1: Temperature*, edited by S. Levitus, 182 pp., U.S. Govt. Print. Off., Washington, D.C.

Locarnini, R. A., A. V. Mishonov, J. I. Antonov, T. P. Boyer, H. E. Garcia, O. K. Baranova, M. M. Zweng, and D. R. Johnson (2010), *World Ocean Atlas 2009, Volume 1: Temperature*, edited by S. Levitus, 184 pp., U.S. Govt. Print. Off., Washington, D.C.

Longshore, D. (2008), *Encyclopedia of Hurricanes, Typhoons, and Cyclones*, 468 pp., Checkmark, New York.

Lukas, R., and E. Lindstrom (1991), The mixed layer of the western equatorial Pacific, *J. Geophys. Res.*, *96*, 3343–3357.

Madec, G. (2008), NEMO ocean engine, *Note Pôle Modél. 27*, Inst. Pierre-Simon Laplace, Paris.

Mainelli, M., M. DeMaria, L. K. Shay, and G. Goni (2008), Application of oceanic heat content estimation to operational forecasting of recent Atlantic category 5 hurricanes, *Weather Forecast.*, *23*, 3–16, doi:10.1175/2007WAF2006111.1.

Marks, F. D., and L. K. Shay (1998), Landfalling tropical cyclones: Forecast problems and associated research opportunities, *Bull. Am. Meteorol. Soc.*, *79*, 305–323.

Marsaleix, P., F. Auclair, J. W. Floor, M. J. Herrmann, C. Estournel, I. Pairaud, and C. Ulses (2008), Energy conservation issues in sigma-coordinate free-surface ocean models, *Ocean Modell.*, *20*, 61–89, doi:10.1016/j.ocemod.2007.07.005.

McPhaden, M. J., G. R. Foltz, T. Lee, V. S. N. Murty, M. Ravichandran, G. A. Vecchi, J. Vialard, J. D. Wiggert, and L. Yu (2009), Ocean-atmosphere interactions during cyclone Nargis, *Eos Trans. AGU*, *90*, 53–54, doi:10.1029/2009EO070001.

Mellor, G., and A. Blumberg (2004), Wave breaking and ocean surface layer thermal response, *J. Phys. Oceanogr.*, *34*, 693–698, doi:10.1175/2517.1.

Menkes, C. E., M. Lengaigne, P. Marchesiello, N. Jourdain, E. M. Vincent, J. Lefèvre, F. Chauvin, and J.-F. Royer (2012), Comparison of tropical cyclogenesis indices on seasonal to interannual timescales, *Clim. Dyn.*, *38*, 301–321, doi:10.1007/s00382-011-1126-x.

Muller-Karger, F. E., P. L. Richardson, and D. McGillicuddy (1995), On the offshore dispersal of the Amazon's plume in the North Atlantic, *Deep Sea Res., Part I*, *42*, 2127–2137, doi:10.1016/0967-0637(95)00085-2.

Nidheesh, A. G., M. Lengaigne, J. Vialard, A. S. Unnikrishnan and H. Dayan (2012) Decadal variability in the tropical Indo-Pacific region: General Circulation Models analysis, *Clim. Dyn.*, doi:10.1007/s00382-012-1463-4, in press.

Papa, F., F. Durand, W. B. Rossow, A. Rahman, and S. Bala (2010), Satellite altimeter-derived monthly discharge of the Ganga-Brahmaputra River and its seasonal to interannual variations from 1993 to 2008, *J. Geophys. Res.*, *115*, C12013, doi:10.1029/2009JC006075.

Penduff, T., M. Juza, L. Brodeau, G. C. Smith, B. Barnier, J.-M. Molines, A.-M. Treguier, and G. Madec (2010), Impact of global ocean model resolution on sea-level variability with emphasis on interannual time scales, *Ocean Sci.*, *6*, 269–284, doi:10.5194/os-6-269-2010.

Prasad, T. G. (1997), Annual and seasonal mean buoyancy fluxes for the tropical Indian Ocean, *Curr. Sci.*, *73*(8), 667–674.

Price, J. F. (1981), Upper ocean response to a hurricane, *J. Phys. Oceanogr.*, *11*, 153–175, doi:10.1175/1520-0485(1981)011<0153:UORTAH>2.0.CO;2.

Rao, R. R. (1987), Further analysis on the thermal response of the upper Bay of Bengal to the forcing of the pre-monsoon cyclonic storm and summer monsoonal onset during MONEX-79, *Mausam*, *38*(2), 147–156.

Rao, R. R., and R. Sivakumar (2003), Seasonal variability of sea surface salinity and salt budget of the mixed layer of the north Indian Ocean, *J. Geophys. Res.*, *108*(C1), 3009, doi:10.1029/2001JC000907.

Rao, S. A., and S. K. Behera (2005), Subsurface influence on SST in the tropical Indian Ocean: Structure and interannual variability, *Dyn. Atmos. Oceans*, *39*(1–2), 103–135, doi:10.1016/j.dynatmoce.2004.10.014.

Riehl, H. (1950), A model of hurricane formation, *J. Appl. Phys.*, *21*, 917–925, doi:10.1063/1.1699784.

Schade, L. R. (2000), Tropical cyclone intensity and sea surface temperature, *J. Atmos. Sci.*, *57*, 3122–3130, doi:10.1175/1520-0469(2000)057<3122:TCIASS>2.0.CO;2.

Sengupta, D., G. N. Bharath Raj, and S. S. C. Shenoi (2006), Surface freshwater from Bay of Bengal runoff and Indonesian throughflow in the tropical Indian Ocean, *Geophys. Res. Lett.*, *33*, L22609, doi:10.1029/2006GL027573.

Sengupta, D., R. G. Bharath, and D. S. Anitha (2008), Cyclone-induced mixing does not cool SST in the post-monsoon north Bay of Bengal, *Atmos. Sci. Lett.*, *9*, 1–6, doi:10.1002/asl.162.

Shay, L. K., and J. K. Brewster (2010), Oceanic heat content variability in the eastern Pacific Ocean for hurricane intensity forecasting, *Mon. Weather Rev.*, *138*, 2110–2131, doi:10.1175/2010MWR3189.1.

Shay, L. K., P. Black, A. Mariano, J. Hawkins, and R. Elsberry (1992), Upper ocean response to hurricane Gilbert, *J. Geophys. Res.*, *97*(20), 227–248.

Shay, L. K., G. J. Goni, and P. G. Black (2000), Effects of a warm oceanic feature on Hurricane Opal, *Mon. Weather Rev.*, *128*, 1366–1383, doi:10.1175/1520-0493(2000)128<1366:EOAWOF>2.0.CO;2.

Shenoi, S. S. C., D. Shankar, and S. R. Shetye (2002), Differences in heat budgets of the near-surface Arabian Sea and Bay of Bengal: Implications for the summer monsoon, *J. Geophys. Res.*, *107*(C6), 3052, doi:10.1029/2000JC000679.

Shenoi, S. S. C., et al. (2005), Hydrography and water masses in the southeastern Arabian Sea during March–June 2003, *J. Earth Syst. Sci.*, *114*, 475–491, doi:10.1007/BF02702024.

Shetye, S. R., S. S. C. Shenoi, A. D. Gouveia, G. S. Michael, D. Sundar, and G. Nampoothiri (1991), Wind-driven coastal upwelling along the western boundary of the Bay of Bengal during the southwest monsoon, *Cont. Shelf Res.*, *11*, 1397–1408, doi:10.1016/0278-4343(91)90042-5.

Shetye, S. R., A. D. Gouveia, D. Shankar, S. S. C. Shenoi, P. N. Vinayachandran, D. Sundar, G. S. Michael, and G. Nampoothiri (1996), Hydrography and circulation in the western Bay of Bengal during the northeast monsoon, *J. Geophys. Res.*, *101*, 14,011–14,025, doi:10.1029/95JC03307.

Sprintall, J., and M. Tomczak (1992), Evidence of barrier layer in the surface layer of tropics, *J. Geophys. Res.*, *97*, 7305–7316, doi:10.1029/92JC00407.

Subrahmanyam, B., V. S. N. Murty, R. J. Sharp, and J. J. O'Brien (2005), Air-sea coupling during the Tropical Cyclones in the Indian Ocean: A case study using satellite observations, *Pure Appl. Geophys.*, *162*, 1643–1672, doi:10.1007/s00024-005-2687-6.

Thadathil, P., P. M. Muraleedharan, R. R. Rao, Y. K. Somayajulu, G. V. Reddy, and C. Revichandran (2007), Observed seasonal variability of barrier layer in the Bay of Bengal, *J. Geophys. Res.*, *112*, C02009, doi:10.1029/2006JC003651.

Vinayachandran, P. N., V. S. N. Murty, and V. R. Babu (2002), Observations of barrier layer formation in the Bay of Bengal during summer monsoon, *J. Geophys. Res.*, *107*(C12), 8018, doi:10.1029/2001JC000831.

Vinayachandran, P. N., T. Kagimoto, Y. Masumoto, P. Chauhan, S. R. Nayak, and T. Yamagata (2005), Bifurcation of the East India Coastal Current east of Sri Lanka, *Geophys. Res. Lett.*, *32*, L15606, doi:10.1029/2005GL022864.

Vincent, E. M., M. Lengaigne, G. Madec, J. Vialard, G. Samson, N. Jourdain, C. E. Menkes, and S. Jullien (2012a), Processes setting the characteristics of sea surface cooling induced by tropical cyclones, *J. Geophys. Res.*, *117*, C02020, doi:10.1029/2011JC007396.

Vincent, E. M., M. Lengaigne, J. Vialard, G. Madec, N. Jourdain, and S. Masson (2012b), Assessing the oceanic control on the amplitude of sea surface cooling induced by tropical cyclones, *J. Geophys. Res.*, *117*, C05023, doi:10.1029/2011JC007705.

Vincent, E. M., G. Madec, M. Lengaigne, A. Koch-Larrouy, J. Vialard (2012c) Influence of Tropical Cyclones on sea surface temperature seasonal cycle and ocean heat transport. *Clim. Dyn.*, 10.1007/s00382-012-1556-0, in press.

Wang, B., Q. Ding, and P. V. Joseph (2009), Objective definition of the Indian Summer Monsoon Onset, *J. Climate*, *22*, 3303–3316, doi:10.1175/2008JCLI2675.1.

Wang, J.-W., W. Han, and R. L. Sriver (2012a), Impact of tropical cyclones on the ocean heat budget in the Bay of Bengal during 1999. Part I: Model configuration and evaluation, *J. Geophys. Res.*, *117*, C09020, doi:10.1029/2012JC008372.

Wang, J.-W., W. Han, and R. L. Sriver (2012b), Impact of tropical cyclones on the ocean heat budget in the Bay of Bengal during 1999. Part II: Processes and interpretations, *J. Geophys. Res.*, *117*, C09021, doi:10.1029/2012JC008373.

Webster, P. J. (2008), Myanmar's deadly "daffodil," *Nat. Geosci.*, *1*, 488–490, doi:10.1038/ngeo257.

Weinkle, J., R. Maue, and R. Pielke (2012), Historical global tropical cyclone landfalls, *J. Clim.*, *25*, 4729–4735, doi:10.1175/JCLI-D-11-00719.1.

Wentz, F. J., C. Gentemann, D. Smith, and D. Chelton (2000), Satellite measurements of sea surface temperature through clouds, *Science*, *288*, 847–850, doi:10.1126/science.288.5467.847.

Willoughby, H. E., R. W. R. Darling, and M. E. Rahn (2006), Parametric representation of the primary hurricane vortex. Part II: A new family of sectionally continuous profiles, *Mon. Weather Rev.*, *134*, 1102–1120, doi:10.1175/MWR3106.1.

Yablonsky, R. M., and I. Ginis (2009), Limitation of one-dimensional ocean models for coupled hurricane-ocean model forecasts, *Mon. Weather Rev.*, *137*, 4410–4419, doi:10.1175/2009MWR2863.1.

Yu, L., and M. J. McPhaden (2011), Ocean preconditioning of Cyclone Nargis in the Bay of Bengal: Interaction between Rossby waves, surface fresh waters, and sea surface temperatures, *J. Phys. Oceanogr.*, *41*, 1741–1755, doi:10.1175/2011JPO4437.1.